International Journal of Nanomedicine

Dovepress
open access to scientific and medical research

Open Access Full Text Article

ORIGINAL RESEARCH

Coaxial Electrospun Polycaprolactone/Gelatin Nanofiber Membrane Loaded with Salidroside and Cryptotanshinone Synergistically Promotes Vascularization and Osteogenesis

Xiaoyu Wu[1,2], Chun Liu[2], Yuqing Jiang[2], Ting Dai[1,2], Linxiang Zhang[1,2], Jiafeng Wang[1,2], Hongbin Zhao[1,2]

[1]Gansu Provincial Maternity and Child-Care Hospital, Gansu Provincial Central Hospital, Gansu, People's Republic of China; [2]Changzhou Medical Center, The Affiliated Changzhou Second People's Hospital of Nanjing Medical University, Changzhou, People's Republic of China

Correspondence: Hongbin Zhao, Gansu Provincial Maternity and Child-care Hospital, Gansu Provincial Central Hospital, Gansu, 730070, People's Republic of China, Email zhao761032@163.com

Background: Salidroside (SAL) is the most effective component of *Rhodiola rosea*, a traditional Chinese medicine. Cryptotanshinone (CT) is the main fat-soluble extract of *Salvia miltiorrhiza*, exhibiting considerable potential for application in osteogenesis. Herein, a polycaprolactone/gelatin nanofiber membrane loaded with CT and SAL (PSGC membrane) was successfully fabricated via coaxial electrospinning and characterized.

Methods and Results: This membrane capable of sustained and controlled drug release was employed in this study. Co-culturing the membrane with bone marrow mesenchymal stem cells and human umbilical vein endothelial cells revealed excellent biocompatibility and demonstrated osteogenic and angiogenic capabilities. Furthermore, drug release from the PSGC membrane activated the Wnt/β-catenin signaling pathway and promoted osteogenic differentiation and vascularization. Evaluation of the membrane's vascularization and osteogenic capacities involved transplantation onto a rat's subcutaneous area and assessing rat cranium defects for bone regeneration, respectively. Microcomputed tomography, histological tests, immunohistochemistry, and immunofluorescence staining confirmed the membrane's outstanding angiogenic capacity two weeks post-operation, with a higher incidence of osteogenesis observed in rat cranial defects eight weeks post-surgery.

Conclusion: Overall, the SAL- and CT-loaded coaxial electrospun nanofiber membrane synergistically enhances bone repair and regeneration.

Keywords: gelatin, coaxial electrospinning, vascularization and bone regeneration

Introduction

Treating bone anomalies due to trauma, bone cancer, and other disorders has been a challenging clinical issue. Such treatment often requires extensive bone regeneration and complex procedures. Autologous bone grafting, the "gold standard" for treating bone defects, has potential drawbacks such as donor site deficiencies, limited sources, and sometimes weaker grafted bone.[1–3] Tissue engineering with bionanomaterials supports tissue regeneration by enhancing cell recruitment, adhesion, and differentiation. Additionally, using drugs that regulate cell activity can also speed up the process.

Using biomaterials loaded with growth factors or drugs to promote tissue regeneration is a key focus in tissue engineering. While materials loaded with growth factors like bone morphogenetic proteins and vascular endothelial growth factor (VEGF) show good effects, they have drawbacks such as high cost and short half-lives due to inactivation during fabrication. Conversely, loading biomaterials with drugs has advantages like lower cost and reduced susceptibility to degradation. Thus, loading tissue engineering biomaterials with drugs is an effective method. Surface-modified drug release systems of nanofiber materials reportedly enhance osteogenesis and angiogenesis. Due to their mimetic properties of the bone's basic structure,

Received: 24 January 2024
Accepted: 10 June 2024
Published: 27 June 2024

nanofiber membranes have been reported to promote osteogenic cell differentiation and mineralization.[4] Additionally, these membranes facilitate the delivery of bioactive agents to enhance the osteogenesis of mesenchymal stem cells (MSCs).[5] Growth factors,[6] synthetic drugs,[7] and natural compounds[8] have all been integrated into nanofiber membranes to improve osteogenicity and bone regeneration. Nevertheless, the tiny pore sizes of standard two-dimensional nanomaterials often inhibit cellular penetration throughout the membrane, limiting their applicability in biomedical applications.[9] However, combining diverse materials can considerably compensate for the distinct shortcomings of individual nanomaterials. It is widely known that the structure and composition of electrospun nanofiber are key factors involved in enhancing the mechanical strength and drug-loading/release properties of the nanofiber membrane.[10,11] For example, Tawfik et al reported that coaxial electrospun nanofiber membranes might show delayed release for two drugs.[12] Chen et al encapsulated the antimicrobial agent roxithromycin (ROX) in PCL/poly (lactic acid) (PLA) core–shell porous drug-carrying nanofibers, which delayed the phenomenon of sudden drug release, facilitated slow drug release, and enhanced hydrophobic drug solubility.[13] Peng et al reported that PCL/gelatin-derived coaxial electrospun nanofiber cellulose membranes constantly release the active factor loaded onto them (Mg^{2+} in the reported study), which can help accelerate cell differentiation into osteogenic cells.[14] Therefore, the coaxial electrospun nanofiber technology used in this study offers significant advantages for drug release. The core–sheath structure created via coaxial electrospinning is a useful substitute for encapsulating therapeutic pharmaceutical drugs in polymeric nanofiber membranes and safeguarding the drugs during loading and release. Furthermore, two distinct drugs can be loaded into the core and sheath structures respectively and released through the coaxial nanofiber membrane either synchronously or asynchronously.[15–17] In addition, coaxial electrostatic spinning offers configurable kinetics for macromolecule release from the core, thereby reducing the initial burst problem. Some typical nonelectrospinnable materials can be electrospun if they are entrapped by nearby electrospinnable materials.[18]

Salidroside (SAL) is the most effective component of *Rhodiola rosea*, a traditional Chinese medicine. Numerous studies involving SAL have reported its diverse applications and pharmacological benefits, including antifatigue, antiaging, immunomodulatory, oxygen free–radical scavenging, and anticancer properties.[19–21] Cryptotanshinone (CT) is the main fat-soluble extract of *Salvia miltiorrhiza* and a monomer with anti-inflammatory and antimicrobial properties that demonstrates considerable promise for application in osteogenesis. Previous studies have reported that CT can protect against pulmonary fibrosis by inhibiting the Smad and STAT3 signaling pathways.[22]

Osteogenic differentiation is a tightly controlled process governed by numerous signaling pathways.[23] During osteogenesis, the Wnt/β-catenin signaling pathway controls osteogenesis and bone production.[24] Previous research has revealed that SAL influences mesenchymal stem cell differentiation to neurons via the Wnt/β-catenin and calcium ion signaling pathways.[25] Additionally, SAL promotes the osteogenic differentiation of adipose stromal cells through the Wnt/β-catenin signaling pathway.[26] Furthermore, SAL promotes angiogenesis and demonstrates the potential to accelerate fracture healing.[27,28]

CT exhibits considerable potential for osteogenesis and can treat postmenopausal osteoporosis.[29] Therefore, we hypothesized that the coaxial electrospinning technique can be used to obtain a core–shell-structured nanofiber membrane loaded with SAL (shell) and CT (core). The coaxial electrospun membrane via the activating effect of SAL on the Wnt/β-catenin signaling pathway and the role of CT in osteogenesis, which can promote mesenchymal stem cells (MSCs) differentiate into osteogenesis, angiogenesis, and further enhance bone regeneration.

Based on this hypothesis, we successfully fabricated a PCL/gelatin nanofiber membrane loaded with SAL and CT via the coaxial electrospinning technique. Via drug release from the PSGC membrane activates the Wnt/β-catenin signaling pathway, synergistically enhancing vascularization and bone regeneration. This novel nanofiber membrane has the potential for clinical application as a bone-substituted material.

Materials and Methods

Preparation of the Coaxial Electrospun Nanofibers

As the shell layer solution, 8.5 wt % gelatin (gum strength ~250 g Bloom, Aladdin, Shanghai, China) was dissolved in hexafluoroisopropanol (HFIP, purity > 99.5%, Aladdin, Shanghai, China). As the core layer solution, 8 wt % PCL (MW: 80 kDa, Aladdin, Shanghai, China) was dissolved in HFIP/N, N-dimethylformamide (DMF; ACS spectroscopic grade, purity ≥ 99.8%, Aladdin, Shanghai, China) mixture (4:1 by volume). The prepared core and shell layer solutions were

divided into two 10 mL syringes, respectively, and the syringes were articulated with electrostatic spinning needles corresponding to the core layer injection port and shell layer injection port. To prepare nanofibers loaded with SAL (purity ≥ 98%, Aladdin, Shanghai, China), 0.6 mg of SAL was added to the 20 mL prepared core layer solution with magnetic stirring for 12 h. As for the preparation of nanofiber membranes loaded with CT (purity ≥ 98%, Aladdin, Shanghai, China), the chloroform solution of 1.5 mg CT was added into the 50 mL prepared shell layer solution. Primary micropump (core layer) speed was 0.0006 mm/s, secondary micropump (shell layer) speed was 0.0015 mm/s, low-speed receiver rotational speed was 50.0 r/min, high-voltage direct current power supply was 22.0 kV, and moving platform speed was 5.0 mm/s in the electrostatic spinning apparatus (Yunfan, Tianjin, China). The low-speed receiver was 12 cm away from the coaxial electrospinning pillow. Coaxial electrostatic spinning needles with 17G (inner diameter) - 22G (outer diameter) size. The conditions used for all coaxial electrospinning procedures were 25 °C and 50% ± 5% humidity. Aluminum foil was removed from the surface of the flat receiver used to collect the coaxial electrospun filaments, and it was then placed in a freeze dryer for 24 h to evaporate any remaining organic solvent. The following groups were created from the core–shell nanofibers produced by coaxial electrostatic spinning: (1) PCL/Gelatin named PG; (2) PCL/SAL/Gelatin named PSG; (3) PCL/Gelatin/CT named PGC; (4) PCL/SAL /Gelatin/CT named PSGC.

Morphology and Characterization of the Coaxial Electrospun Nanofiber Membranes

Scanning Electron Microscopy and Fluorescence Microscope Observation

The nanofiber film was cut into 4-cm^2 squares. Then, the film sections were placed on a copper column and their surfaces were sprayed with gold for an hour. The appearance and microstructure of the coaxial electrospun nanofiber membrane were examined using scanning electron microscope (SEM). ImageJ software (National Institutes of Health, USA) was employed to determine the nanofiber sizes. Origin 2021 (Microcal Inc., USA) was used to plot the histograms. Using a fluorescence microscope, the core–shell structure of the coaxial electrospun nanofiber was examined.

Porosity of the Coaxial Electrospun Nanofiber Membranes

The specific gravity method was used to determine the porosity of the membranes. Then, an appropriate amount of anhydrous ethanol was added into a specific gravity bottle (which was equal to the volume of material that can be submerged) and the bottle containing anhydrous ethanol was weighed (W_1). Next, the membrane was cut into 1-cm^2 squares and weighed (W_0). The membrane was then added to the anhydrous ethanol in the specific gravity bottle. Subsequently, the bottle was pumped with vacuum to ensure that the anhydrous ethanol was sufficiently absorbed into the membrane′s pores. Then, the bottle was weighed again (W_2), following which the membranes were removed. Next, the bottle containing anhydrous ethanol was weighed (W_3). These steps were repeated thrice to record the experimental data. The porosity of the sample membrane was calculated using the following formula:[30]

$$P = \frac{W_2 - W_3 - W_0}{W_1 - W_3} \times 100\%$$

Water Contact Angle of the Coaxial Electrospun Nanofiber Membranes

The OCA-20 contact angle system (Feldstadt, Germany) was used to determine the hydrophilicity of the coaxial electrospun nanofiber membrane. After cutting the membranes into 1-cm^2 squares, they were placed on a test carrier. Then, a particular amount of deionized (DI) water was added to the surface of the test sample using the instrument tip after adjusting the field of view. The device determined the water contact angle after 10s. The contact angle was determined thrice for each group.

Air Permeability of the Coaxial Electrospun Nanofiber Membranes

The area of the mouth of the specific gravity bottle was measured beforehand and recorded as S. A suitable quantity of DI water was added to the specific gravity bottle, and three replications were set up for the control and experimental populations. The mouth of the bottle was covered entirely with the material in the experimental population, whereas it was left open in the control population. The weight of the bottles at this point in time was weighed and recorded as m_1,

and after being placed at 37 °C for 24 h, it was noted as m_0. The following formula was used to determine the permeability of the membrane:

$$T = \frac{(m_1 - m_0) \times 10^4}{S \times 24}$$

The permeability of the membrane was determined using the following formula:

$$\text{Permeability}\,(\%) = \frac{T_{test}}{T_{control}} \times 100\%$$

where T_{test} is the experimental group that fixes the electrospun nanofiber membranes at the mouth of the specific gravity bottle and $T_{control}$ is the control group for open-top specific gravity flasks.

Water Absorption Expansion Rate of the Coaxial Electrospun Nanofiber Membranes

Three parallel samples were collected from each group of coaxial electrospun membranes. These samples were immersed in DI water for 24 h, removed, and then placed on a filter paper to absorb the surface moisture. Their initial weight was recorded as m_1. Subsequently, the samples were placed in a perpetually warm dryer at 37 °C for 24 h and then weighed again and recorded as m_2. This process was repeated thrice in total.[31]

$$\text{Water absorption expansion rate}(\%) = \frac{m_1 - m_2}{m_2} \times 100\%$$

Biodegradation Rate of the Coaxial Electrospun Nanofiber Membranes

The sterilized PG group membranes were cut into 1-cm^2 square films and weighed as W_1. Next, the sample was placed in a 50-mL centrifuge tube to which 40 mL of phosphate-buffered saline (PBS) solution was added and then gently shaken in a 37 °C shaker. At 3, 5, 7, 14, and 21 days, the samples were extracted, washed using DI water, lyophilized, and weighed as W_2. The experiment was conducted in triplicate. The biodegradation rate of the membranes was determined using the following formula:[32]

$$\text{Biodegradation rate}(\%) = \frac{W_1 - W_2}{W_1} \times 100\%$$

Mechanical Properties Testing of the Coaxial Electrospun Nanofiber Membranes

Tensile property testing is performed using the universal testing machine (MTS 4204, China). The PSGC group's nanofiber membrane was sliced into 5-cm^2 square films, and the test specimen was put between two fixtures on the microforce tester while being fitted with a 20 kN weight cell at both ends, exposing a surface area of 4 cm^2. The top fixture was then tensile tested at a 3 mm/min rate up to the breaking point three times, and a tensile force–deformation curve was obtained.

X-Ray Diffraction and Fourier-Transform Infrared Spectroscopy Assays

The primary technique for determining the physical phase and crystal structure of a substance is via X-ray diffraction (XRD) (Riguku, D/max-2500, Japan). The diffraction patterns of each set of nanofiber membranes were made with an XRD that scanned the samples from 5° to 80° in steps of about 0.167° in fixed-time mode. The composition of the functional groups in the nanofiber materials was evaluated using Fourier-transform infrared spectroscopy (FTIR). Square films of 1 cm^2 were cut from the different coaxial electrospun supports and put into a Nicolette NEXUS spectrometer. Results for the spectral region of 400–4500 cm^{-1} were obtained with a resolution of 4 cm^{-1}.

In vitro Drug Cumulative Release Measurement

The coaxial electrospun nanofiber films PSGC were cut into 4 cm^2 squares, weighed, and then deposited in 50 mL centrifuge tubes. 30 mL of PBS (0.2 M, pH = 7.4) was added, and the tubes were then placed in a 37 °C shaker with gentle shaking. Every 1 h, 2 h, 4 h, 8 h, 12 h, 1 day, 4 days, 7 days, 10 days, 14 days, 21 days, and 28 days, 1 mL of supernatant from the sample was taken and put in a 1.5 mL centrifuge tube at −20 °C. Then, three parallel samples were

prepared for each group, with equal amounts of supernatant removed and PBS added back. After that, the maximum absorption peaks of SAL at 276 nm and CT at 450 nm were measured by ultraviolet spectrophotometer (Shimadzu Corporation, Japan). Therefore, 276 nm and 450 nm were chosen as the detection wavelengths of these two drugs. To create the standard curve, the absorbance at the corresponding wavelengths of the two drugs was measured in the appropriate concentration range. In this case, SAL was dissolved in 1 mL of PBS and 1 mL of anhydrous ethanol, and CT was dissolved in 1 mL of PBS and 1 mL of chloroform. For testing the slow release of SAL drugs, the removed fluids of the PSGC coaxial fiber were mixed with 1 mL of anhydrous ethanol, and for testing the slow release of CT drugs, the removed fluids were mixed with 1 mL of chloroform, and the absorbance values at the corresponding wavelengths were measured. The drug′s cumulative release rate is determined using the standard curve and the drug′s cumulative release rate equation, as shown below:[33]

$$\text{Cumulative percentage released}\,(\%) = \frac{V1Cn + V2\Sigma C(n-1)}{w} \times 100$$

Cn denotes the concentration of SAL or CT eliminated at each time point. V1 represents the overall volume of PBS (30 mL), whereas V2 reflects the amount of PBS extracted at each interval (1 mL). Furthermore, w denotes the total mass of SAL or CT drug loaded by the nanofibers placed into the centrifuge tube.

Cell Adhesion Assay

The 2 cm^2 ethylene oxide–sterilized nanofiber membrane was put into a 6-well plate, and 1×10^4 mouse bone marrow mesenchymal stem cells (BMSCs, CRL-12424, ATCC, USA) were incubated on it. BMSCs were grown in a medium called complete medium (Dulbecco′s Modified Eagle Medium [DMEM], Gobico, USA) that had 10% fetal bovine serum (FBS, Biological Industries, Israel) and 1% penicillin–streptomycin (Life Technologies Corporation, USA). After adding enough complete medium to just touch the fiber membrane, the 6-well plate was shaken to equally disperse the cells. 37 °C and 5% CO_2 were used to incubate the plates. Following the observation that the cells had adhered to the wall after 4 h, the medium was added to 2 mL dropwise, and the incubation was continued. The 6-well plates were removed on day 3, the medium was aspirated and washed twice with 1 mL of PBS, and the plates were fixed with 500 μL of paraformaldehyde (4%) for 30 min. The plates were dehydrated for 15 min with a gradient of 70%, 80%, 90%, 95%, and 100% ethanol, respectively. To eliminate extra ethanol, the dehydrated membranes were placed in a ventilated kitchen overnight. SEM was used to evaluate cell adhesion to the membrane surface.

Cytoskeleton Observation

Coverslips with a diameter of 14 mm were placed in 12-well plates alongside the membrane films from each group. BMSCs were placed in the well at a concentration of 5×10^3 cells/mL, and 500 μL DMEM was added to each well. For each group, two sets of wells were set up. The membranes were cocultured with BMSCs for 3 days at 5% CO_2 and 37 °C, following which they were gently discarded. The 12-well plates were cleaned twice using 500 μL PBS. The, the cells were fixed with 4% paraformaldehyde for 30 min, following which they were washed with 500 μL PBS twice for 10 min each. The cells were subsequently stained for 45 min using the preset Ghost Pen Cyclic Peptide Staining Solution. The staining solution was aspirated and the cells in each well were washed with 500 μL PBS twice. The cells were removed from the coverslips, sealed with a drop of sealing agent (containing DAPI), left to rest for 10 min, and then examined under a fluorescence microscope.

Live/Dead Cell Staining

The biocompatibility of the membranes was assessed using a live/dead staining kit (L-7011; Invitrogen, Eugene, Oregon, USA). Cells were inoculated into 24-well plates (1.5×10^4 cells/well) and cocultured with the membranes for 3 days, subsequently being stained with live and dead reagents. The cells were then observed under a fluorescent microscope (Zeiss, Oberkochen, Germany).

CCK-8 Testing

Cell Counting Kit-8 (CCK-8, Dojindo Kagaku, Japan) was employed to measure cell proliferation. BMSCs (3×10^3) were added to 96-well plates after the cells had attached to the wall (approximately 2 h). The membranes were cut into 0.5 cm^2 and placed in the 96-well plate. The membranes suspended in a complete medium were removed on days 1, 3, and 5, respectively, and the supernatant was collected after 1 h. A microplate reader (Epoch, Bio Tek, USA) was employed to quantify absorbance at 450 nm.

5-Ethynyl-2'-Deoxyuridine (EdU) Staining

EdU was purchased from Beijing Solarbio Technology Corporation. Human umbilical vein endothelial cells (HUVECs; Zhongqiao Xinzhou, Shanghai, China) were put in 12-well plates for 3 days on cell crawl coverslips with coaxial electrospun membranes of each group and then taken out. Endothelial cell–specific basal medium (Zhongqiao Xinzhou, Shanghai, China) with FBS, endothelial cell growth factor, and penicillin/streptomycin solution in the ratio of 100:5:1:1 was used for the culture of HUVECs. The culture medium was discarded, and the cells were stained with an EdU staining kit. DAPI staining and sealing and the staining results were observed and photographed using a fluorescence microscope (Zeiss, Oberkochen, Germany).

Real-Time PCR (qPCR) Analysis

Real-time PCR (qPCR) was conducted to measure the expression of osteogenesis-related genes, including *ALP, COL1, OCN, RUNX2, OPN*, and *OSX*, and Wnt/β-catenin signaling pathway essential genes including *AXIN1, AXIN2, β-catenin, LRP5, LRP6, GSK3β*, and *WNT3A* in BMSCs, and angiogenesis-related genes such as *CD31, PDGF*, and *NOS3* in HUVECs. Recombinant Dickkopf-1 (PeproTech, Rocky Hill, NJ, USA, DKK-1) is a specific inhibitor of the Wnt/β-catenin signaling pathway. Prior to the correspondence experiment, BMSCs were treated with DKK-1. Based on previous studies, DKK-1 was applied at a concentration of 0.5 μg/mL.[34] After the cells and membranes were cocultured for some time, they were extracted using TRIzol (Qiagen, Germany), and 1 μg of RNA was then reverse transcribed into cDNA using the HiScript II Q RT SuperMix (Vazyme Biotech Co., Ltd., China). Finally, the AceQ qPCR SYBR Green Master Mix (Vazyme Biotech Co., Ltd., China) was used for qPCR. The abovementioned assay was performed on a 96-well PCR plate (Nest Biotechnology, Wuxi, China). The $2^{-\Delta\Delta Ct}$ method was used to measure the expression of the target gene. Supplementary Table S1 provides a detailed description of the primers; the qPCR reactions were conducted in triplicate for both the target and the housekeeping gene GAPDH.

Staining with Alkaline Phosphatase and Alizarin Red S

Alkaline phosphatase (ALP) activity and calcium nodule deposition in different membranes were assessed using ALP and alizarin red S (ARS) staining kits. In summary, BMSCs were placed in 6-well plates at a concentration of 3×10^4 cells per well., and cocultured with the coaxial electrospun membranes for 7 and 21 days, respectively, for ALP staining and ARS staining. The staining outcomes were examined using a light microscope and recorded on camera.

Western Blotting

The cultured cells were lysed using RIPA lysis buffer enhanced with proteasome and phosphatase inhibitors. Following lysis, centrifugation was performed to remove the cell debris. Protein concentration was measured using the BCA kit (BCA kit, Beyotime, Shanghai, China). The proteins were separated via sodium dodecyl sulfate–polyacrylamide gel electrophoresis (Vazyme, Nanjing, China) and placed on a polyvinylidene fluoride membrane (Millipore, Shanghai, China). The membranes were incubated with appropriate primary antibodies (mouse polyclonal antibodies VEGF, 1:800 dilution; rabbit monoclonal CD31, 1:800 dilution) overnight at 4 °C. Subsequently, the membranes were incubated with secondary antibodies for 1 h at room temperature. The secondary antibodies used were horseradish peroxidase (HRP)-labeled goat anti-rabbit IgG and HRP-labeled goat anti-mouse IgG (1:1000; Beyotime, Shanghai, China). The signal intensity was evaluated using NcmECL Ultra (New Cell & Molecular Biotech, China) and Bio-Rad XRS chemical luminescence detection device system (Hercules, California, USA).

Cellular Immunofluorescence Staining

The prepared sterile 14-mm-diameter coverslips were placed on a 24-well plate, and cells (2×10^4 cells/well) were added to coculture with the membrane. In addition, 4% paraformaldehyde was used to fix the cells, following which they were treated with 2 mg/mL glycine for 10 min. After that, the cells were incubated in 0.2% Triton X-100 permeabilizing solution for 30 min and in 3% BSA at 4 °C overnight. Following this, the cells were incubated with the primary antibody for 1 h at room temperature, and then eluted using immunofluorescence eluent. The membranes were subsequently incubated at room temperature with the secondary antibody. The membrane films were sealed with a DAPI-containing sealer for 10 min and then observed under the fluorescence microscope to picture the stained slices.

Tube Formation Assay

The substrate glue was selected from ABW in Shanghai, China. A 24-well plate was filled with 120 μL of substrate glue which was distributed equally throughout each well before being incubated at 37 °C for 30 min. In each well, 1×10^5 cells of HUVECs were cocultured with the membranes. The membranes were removed from the well plate after 12 h, and the tube formation of HUVECs was observed under a light microscope.

Enzyme-Linked Immunosorbent Assay

The human VEGF enzyme-linked immunosorbent assay (ELISA) Kit was purchased from Cluster Bio. HUVECs were placed in 6-well plates and cocultured with the membranes for 3 days before the supernatant was collected for analysis. Using the human VEGF ELISA Kit, the optical density values at 450 nm and 570 nm were determined by dual-wavelength detection with an enzyme marker (Epoch, Bio Tek, USA). Standard curves were created, and the findings were statistically examined.

Constructing Bone Defect Animal Model

The animal model constructed in this study is a rat cranial bone defect model, with symmetrical defects of 5 mm created on both sides of the rat skull. All animal experiments comply with relevant animal experimental laws in China and are approved by the Ethics Committee of Nanjing Medical University. The experimental animals are 50 male SD rats weighing 200g-220g. Randomly divide the prepared rats into 5 groups: Control group (10 rats), PG group (10 rats), PSG group (10 rats), PGC group (10 rats), PSGC group (10 rats). The specific construction method is as follows:

After preparing necessary surgical instruments, anesthesia, and disinfectants, the rats are anesthetized. The surface of the skull is then exposed by making an incision on the rat's head and separating the soft tissues. Using an orthopedic drill, two symmetrical defects of approximately 5 mm in diameter are created on each side of the rat's head. The sterile nanofiber membrane is placed on the defect site, covering the exposed tissue and adhering to the bone defect. After treating the cranial bone defect, the soft tissues are sutured layer by layer to promote proper wound healing. Post-surgery, the animals are cared for, observed, and administered necessary medication to monitor their recovery. Finally, after 8 weeks of normal feeding, the cranial bones are removed and preserved in formalin fixative for examination of the growth at the defect site.

Constructing Vascularized Animal Model

To begin, prepare the necessary experimental materials, ensuring a sterile environment. Then, use appropriate anesthesia methods to ensure the rats are pain-free. An incision was made on the back of the rats centered on the spine, and four subcutaneous pouches were formed two by two symmetrically on the back of each experimental rat. Next, place the pre-prepared nanofiber membranes in the pockets, ensuring contact with the surrounding tissues. Suture the incisions carefully and provide antibiotics and analgesics for the rats' recovery. After 2 weeks and 4 weeks post-surgery, remove the membranes for analysis. Assess the survival and vascularization of the tissues using techniques like staining and microscopy.

Microcomputed Tomography Assay

In high-resolution scanning mode, three-dimensional skull images collected at 4 and 8 weeks were viewed using a micro-CT scanner (SkyScan 1176 In vivo Micro-CT, Bruker, Belgium) to analyze and quantify the new bone. Further investigation was conducted into bone restoration metrics, such as bone volume (BV), bone volume/total volume percentage (BV/TV), and bone trabecular density (Tb.N). All animal experiments were performed in strict accordance with the Nanjing Medical University Animal Ethics Committee guidelines.

Hematoxylin and Eosin and Masson's Trichrome Staining

Rat cranial tissues were fixed with 4% polyformaldehyde, demineralized for 40 days at 37 °C with 15% ethylenediaminetetraacetic acid, paraffin-embedded, and sectioned. The tissues were deparaffinized using an ethanol gradient, histologically stained via hematoxylin and eosin (H&E) and Masson′s trichrome staining, and then observed under a light microscope (Olympus, Japan). ImageJ software (Media Cybernetics, Rockville, MD, USA) was used for the evaluation.

Immunohistochemical and Immunofluorescence Staining

Immunohistochemistry and immunofluorescence were used to detect the expression of osteogenesis-related proteins in the body. Tissue slices were deparaffinized, treated with an antigen repair solution for 15 min at 37 °C, permeabilized with 5% Triton X-100 to inactivate endogenous peroxidase, and added to a 5% BSA blocking buffer. COL1 mouse monoclonal antibody (1:100, Abcam, USA), OSX, OCN (1:100, Santa Cruz, USA) mouse polyclonal antibody, and rabbit polyclonal antibody to RUNX2 (1:200, Proteintech, Wuhan, China) were incubated for 12 h at 4 °C. Subsequently, the slices underwent treatment with a biotinylated goat anti-rabbit/mouse secondary antibody (diluted at 1:200, Beyotime Biotechnology, Shanghai, China) at a temperature of 37 °C for 30 min; afterward, SABC was added for 30 min at 37 °C. Lastly, the sections were treated with 3,3′-diaminobenzidine tetrahydrochloride at room temperature for 5–10 min. For immunofluorescence, the sections were stained directly with the corresponding secondary antibody after incubation with DAPI, and the sections were blocked with an anti-fluorescent attenuating sealer. The samples were then observed under a light microscope (ZEISS, Germany).

Statistical Analysis

The data are expressed as mean ± standard deviation, and data analysis was performed using GraphPad Prism version 9.0 (San Diego, CA, USA). To evaluate statistical significance between groups, one-way analysis of variance was employed. A p-value of <0.05 was considered statistically significant.

Results

SEM and Fluorescence Staining Results of the Coaxial Electrospun Nanofiber Membranes

The coaxial electrospun membranes comprise multiple nanofiber filaments with smooth surfaces (Figure 1a). These nanofibers are continuously linked to form a loose and porous microstructure. As shown in the SEM images (Figure 1b), the structure and morphology of the fibers are identical. The diameter of the coaxial nanofibers was typically between 600 and 1000 nm (Figure 1c).

The core–shell structure of the PG nanofiber membranes was observed using a fluorescence microscope. Green fluorescein sodium and red rhodamine were added to the gelatin and PCL solutions during the fabrication of the coaxial electrospun membranes, respectively. A fluorescence microscope was used to track the distribution of the two dyes. The nanofibers exhibited a core–shell structure as the red rhodamine dye was tightly bound to the core layer while the green fluorescein sodium dye was dispersed around the core layer where PCL was localized (Figure 1d).

Characterization of the Coaxial Electrospun Nanofiber Membranes

Supplementary Figure S1 demonstrates the surface characterization of the different membranes. The porosities of the PG, PSG, PGC, and PSGC membranes were 27.03% ± 2.53%, 29.06% ± 0.82%, 26.72% ± 4.91%, and 25.00% ± 4.08%,

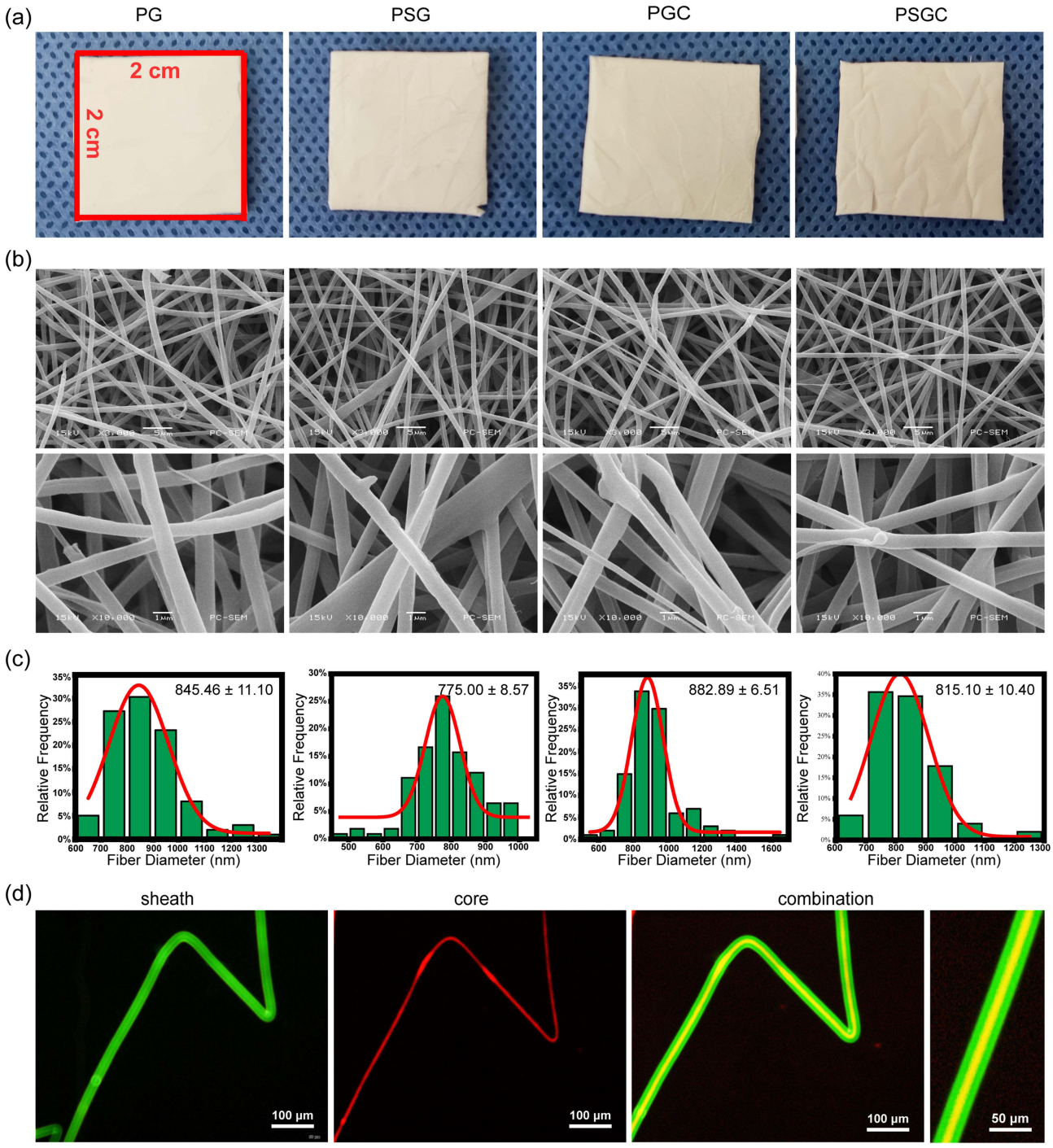

Figure 1 Characterization of four groups of coaxial electrospun membranes at the macroscopic and microscopic levels. (**a**) General observation photographs. (**b**) Images from a SEM. (**c**) Fiber diameter statistics as revealed via SEM. (**d**) Fluorescence images of the core–shell nanofibers; fluorescein sodium (green) and rhodamine (red) indicate the shell and core, respectively. Results are expressed as the mean ± standard deviation (n = 3).
Abbreviation: SEM, scanning electron microscope.

respectively. There was no significant difference between the membranes (Supplementary Figure S1a). The water contact angle results indicated that the membranes had good hydrophilicity (Supplementary Figure S1b). All membranes exhibited excellent air permeability of up to ≥ 67% (Supplementary Figure S1c). The water absorption and expansion of the PG, PSG, PGC, and PSGC membranes were 459.71% ± 12.25%, 460.43% ± 4.15%, 518.52% ± 51.26%, and 467.22% ± 23.99%, respectively (Supplementary Figure S1d). There was no significant difference in the porosity, water

contact angle, permeability, water absorption, or swelling rate among the membranes, suggesting that the addition of SAL and CT did not alter the physical properties of the membranes.

Biodegradation Rate

In our previous study, we reported that loading drugs did not alter the relevant physical properties of membranes thus, we determined the degradation rate using the PG group stents as a representative. Supplementary Figure S1e demonstrates that the membranes exhibited the highest biodegradation rate on day 5 (72.04% ± 0.19%), with the rate gradually stabilizing after 14 days (75.27% ± 1.06%).

Mechanical Properties

The membranes were subjected to tensile tests with a tensile speed of 3 mm/min. As force values increased, the tensile deformation of the membranes gradually increased, with a trend of rapid and then gradual increase. The force–deformation curves of the PG membranes of the membranes for three representative replications at the same stress almost overlapped (Supplementary Figure S1f and g). The average value of the maximum deformation of the membrane was 3.653 mm, and the average value of the maximum force was 17.169 N. Furthermore, the mechanical tensile test revealed that the prepared PG stent exhibited strong ductility.

XRD and FTIR Tests

The XRD pattern is shown in Supplementary Figure S1h. The peak of the PSGC membrane at $2\theta = 26.2°$ is the sharpest, indicating that this membrane exhibited the best crystallinity among the membranes in this place. As shown in the XRD patterns, there is one obvious absorption peak at $2\theta = 21°$ for all the four representative membranes, which indicates the diffraction peak of gelatin, representing its amorphous nature.[35] PCL, a semicrystalline polymer, exhibited absorption peaks in the pattern at $2\theta = 21.57°$ and $2\theta = 23.85°$, wherein one diffracted absorption peak was stronger and the other weaker, consistent with the characteristics of the PCL diffraction peak.[36,37]

The FTIR spectra are shown in Supplementary Figure S1i. The characteristic C=O and C–O absorption peaks of PCL were at 1725 and 1184 cm^{-1}, respectively, and the stronger absorption peaks were at 1650 and 1540 cm^{-1}, corresponding to the amide I band (stretching vibration against the symmetrical carboxyl or C=O group) and the amide II band (C–N stretching or N–H bending vibration), respectively, in the gelatin structure.[38,39] The characteristic absorption peak at 2360 cm^{-1} in the FTIR spectra is the most obvious, caused by the fact that there are more triple and cumulative double bonds in the CT molecule than in the SAL molecule, thereby rendering the absorption peak of the membranes containing CT more obvious than those of the other membranes. In the PSGC membranes, the peaks were more pronounced owing to the presence of CT as well as SAL, resulting in the superposition of triple bonds and cumulative double bonds, than those of the membranes containing only SAL or CT.

In vitro Drug Release Rate

The chemical structures of SAL and CT drugs loaded in the membranes are shown in Figure 2a and b. Their slow-release profiles in the coaxial electrospun nanomembranes are displayed in Figure 2c. In the PSGC membrane, the SAL′s release showed a typical trend of fast and then slow, with a sharp release of SAL in the first 4 days and a stabilization at 14 days, and the final cumulative release rate of SAL was 48.61% ± 7.82% on day 21. Besides, the sustained release of CT was tested with the PSGC membrane, with a burst of the drug release at the beginning of the first 24 h, followed by a period of stable release, and a final cumulative release rate on day 21. The cumulative release rate of CT was higher than that of SAL (Figure 2c).

Cell Proliferation and Morphology of BMSCs on Coaxial Electrospun Nanofiber Membranes

After coculturing BMSCs with the different coaxial electrospun membranes for 3 days, SEM analysis revealed that cells adhered to the membranes′ exterior and interior pores, aggregated into cell clusters, and had well-extended pseudopods,

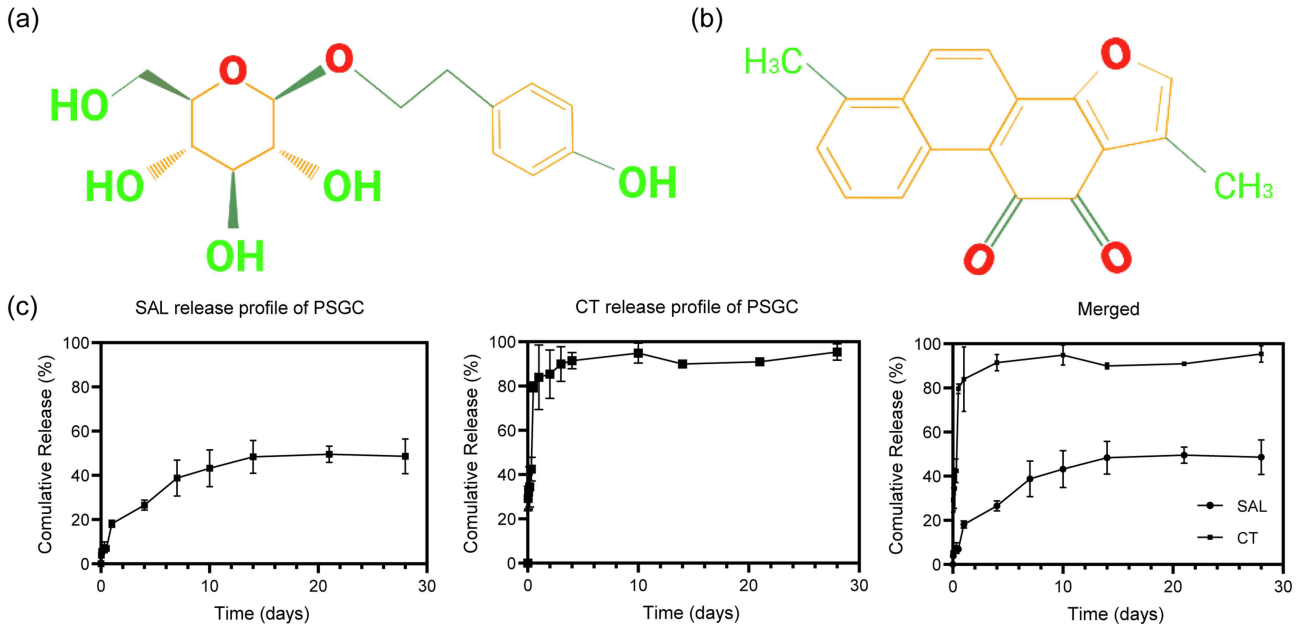

Figure 2 Chemical structural formula of salidroside, cryptotanshinone, and sustained release kinetics of electrospun-loaded SAL and CT in vitro. (**a**) Chemical structures of SAL. (**b**) Chemical structures of CT. (**c**) Cumulative drug release curves of SAL and CT from the PSGC coaxial electrospun membranes, respectively. Results are expressed as the mean ± standard deviation (n = 3).
Abbreviations: SAL, salidroside; CT, cryptotanshinone.

indicating that the membranes were almost completely non-toxic and that their porous design was advantageous for cell growth (Figure 3a). The effect of the membranes on the cytoskeleton was investigated using phalloidin staining, and the results showed that cells on the membrane surface had a complete cytoskeleton. Membranes allow cell pseudopods to expand in preparation for cell proliferation and adherence. Consequently, the addition of the membranes did not affect the cell morphology to a large extent in vitro (Figure 3b). The results of the live/dead cell staining of BMSCs cocultured with the membranes showed that a larger number of live cells (green) could be found, in contrast to only a very smaller number of dead cells (red) on the membranes, indicating the viability of the cells on the membranes and their near-toxin-free nature (Figure 3c). The CCK-8 assay proved that there was no discernible difference among the membranes on day 1. On day 3, the cell proliferation in the PG and PSGC membranes was slightly lower than that of the control group. However, the results on day 5 showed that the cell proliferation was significantly increased as compared with that of 1 and 3 days. Furthermore, there were no significant differences among different membranes (Figure 3d). These findings suggest that the membranes have strong biocompatibility and a low degree of cytotoxicity, which satisfy the fundamental criteria for biomaterials.

Assessing Osteogenic Capacity

The effects of the PG and PSGC membranes on osteogenesis were identified via qPCR analysis and compared with those of the control group after BMSCs were cocultured with each group of membranes for 3, 7, and 14 days. At 3, 7, and 14 days, the osteogenesis-related gene expression levels, such as those of *ALP, COL1, OCN, OPN*, and *OSX*, were upregulated in the PG membrane compared with those in the control group. Furthermore, the expression levels of these genes were considerably higher in the PSGC membranes than in the control group and PG membranes. When co-cultivated for 3 and 7 days, *RUNX2* expression levels drastically increased in the PG and PSGC membranes; however, there was no significant difference in its expression levels in all the membranes after 14 days (Figure 4a). These results suggest that the membranes could control the expression levels of osteogenesis-related genes via drug release. Thus, the PSGC membrane exhibited an excellent osteogenic effect.

Alkaline phosphatase and alizarin red staining were both performed to evaluate the short- and long-term osteogenic differentiation of BMSCs. The number of calcium nodules was considerably higher in the PG membrane than in the

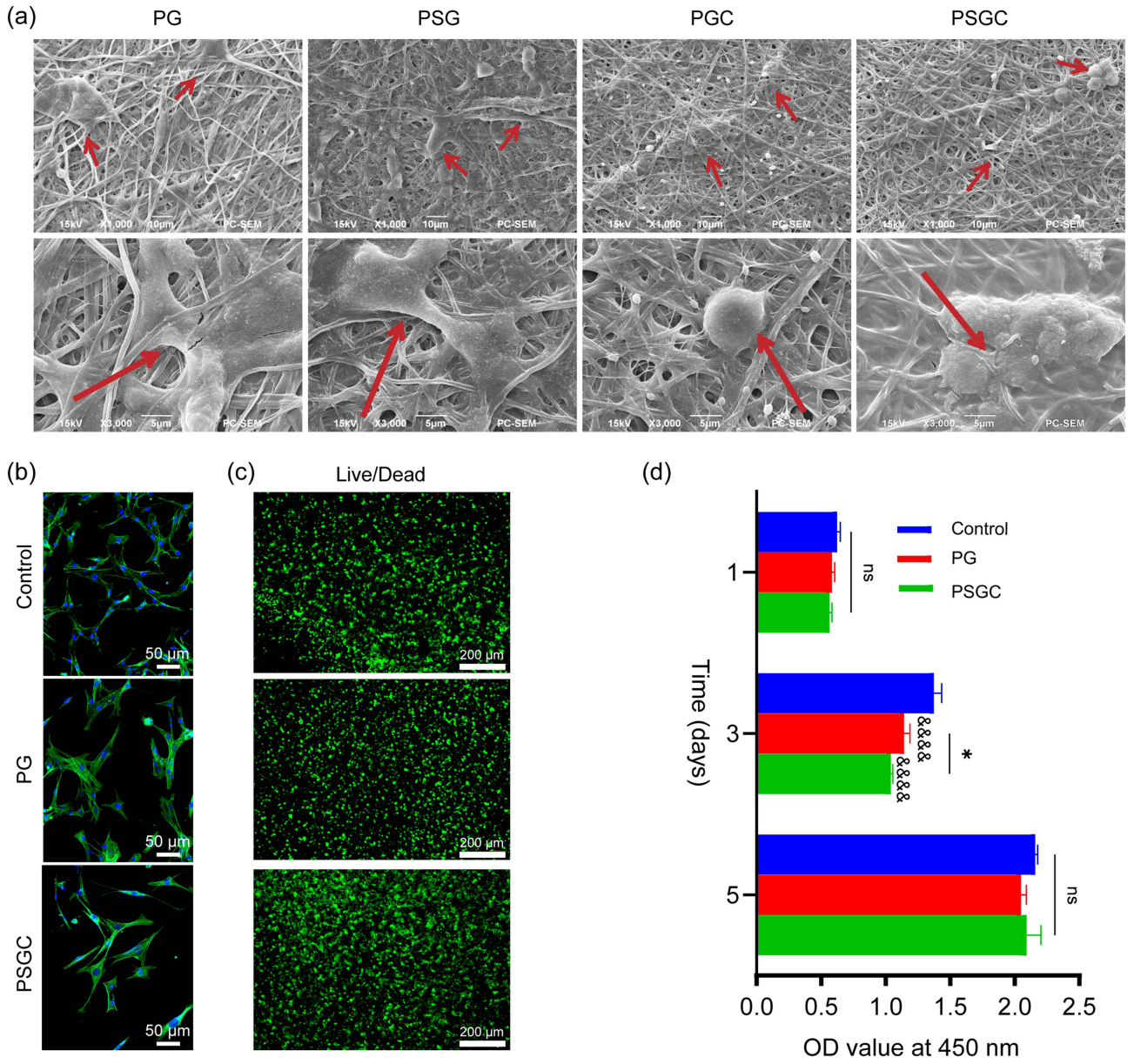

Figure 3 In vitro biocompatibility evaluation of BMSCs cocultured with the different membranes. (**a**) SEM images of cell adhesion on the membranes at 3 days. Red arrows indicate cells. (**b**) Phalloidin staining. (**c**) Live/dead staining: BMSCs were grown together with different types of membranes for 3 days. Red color indicates dead cells, whereas green depicts living ones. (**d**) The outcome of the CCK-8 experiment. Results are expressed as the mean ± standard deviation (n = 3). $^{*}p < 0.05$ and $^{\&\&\&\&}p < 0.0001$ compared to the control group.

Abbreviations: BMSCs, bone marrow mesenchymal stem cells; CCK-8, cell Counting Kit-8.

control group at 21 days. Afterward, a significantly higher number of calcium nodules were detected in the PSGC membranes compared with the PG membrane and control group. The ALP staining results are shown in Figure 4b. The ALP activity in the PG membranes was higher than in the control group. Furthermore, the PSGC membranes exhibited significantly higher ALP activity compared with the PG membrane and control group, indicating that the PSGC membranes could enhance the ALP activity of cells and induce BMSCs to differentiate into osteogenic cells. Figure 4c shows RUNX2 protein expression in the various membranes. The PSGC membranes exhibited substantially higher RUNX2 protein expression compared with the other membranes (Figure 4d).

To further prove the osteogenic effect of the different membranes, a Western blot assay was performed to evaluate the expression of the osteogenesis-related proteins. The results revealed that compared with the control group and PG membranes, the expression levels of the RUNX2 protein in the BMSCs cocultured with the PSGC membranes were

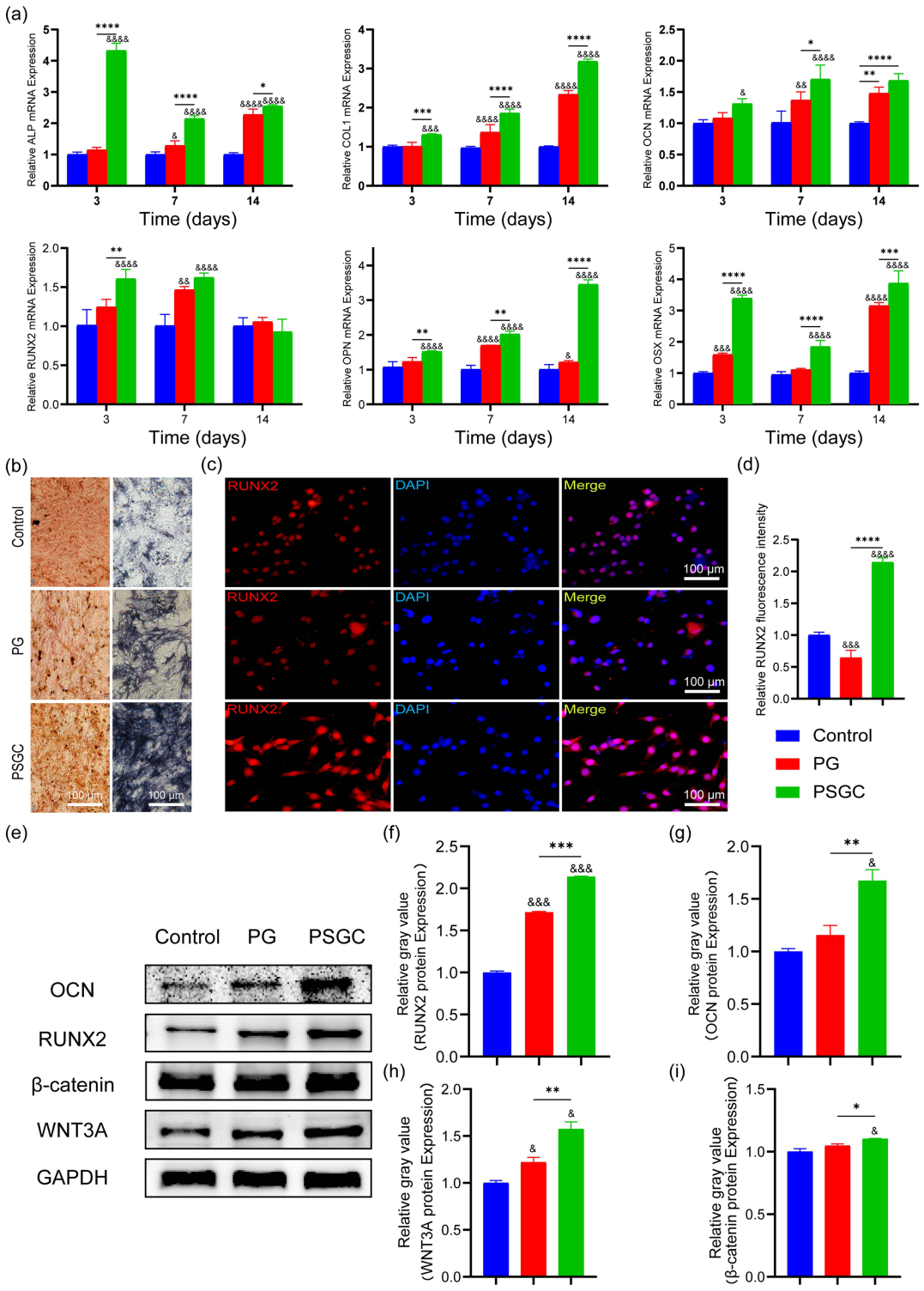

Figure 4 In vitro osteogenic differentiation of BMSCs cocultured with the different nanofiber membranes. (**a**) ALP, COL1, OCN, RUNX2, OPN, and OSX mRNA expression on days 3, 7, and 14. (**b**) ARS and ALP staining results. (**c**) Representative images of the RUNX2 immunofluorescence experiment of BMSCs cocultured with the different nanofiber membranes for 3 days. (**d**) RUNX2 protein expression from (**c**) was quantified. Results are expressed as the mean ± standard deviation (n = 3). (**e**) Western blot assay of osteogenesis-related and Wnt/β-catenin pathway–associated protein expression following coculturing BMSCs with the different membranes for 7 days. (**f** and **g**) Quantitative analyses of *RUNX2* and *OCN* protein expression levels from (**e**). (**h** and **i**) Quantitative analyses of *WNT3A* and *β-catenin* protein expression levels from (**e**). $^{\&}p < 0.05$, $^{\&\&}p < 0.01$, $^{\&\&\&}p < 0.001$, and $^{\&\&\&\&}p < 0.0001$. $^{*}p < 0.05$, $^{**}p < 0.01$, $^{***}p < 0.001$, and $^{****}p < 0.0001$.

Abbreviations: ALP, alkaline phosphatase; COL1, collagen I; OCN, osteonectin; RUNX2, runt-related transcription factor 2; OPN, osteopontin; OSX, osterix; WNT3A, wingless-type MMTV integration site family (member 3A); β-catenin, cadherin-Associated Protein (Beta 1).

significantly higher (Figure 4e and f). Similarly, the expression levels of the OCN protein in the BMSCs cocultured with the PSGC membranes were higher compared with those in the control group and PG membranes (Figure 4e and g). These outcomes reveal that the PSGC membranes could promote osteogenesis-related protein expression and mesenchymal stem cell differentiation.

SAL- and CT-Loaded Coaxial Electrospun Nanofiber Membranes Activate the Wnt/β-Catenin Signaling Pathway

The Wnt/β-catenin signaling pathway considerably impacts the osteogenic transformation of BMSCs. qPCR and Western blotting analyses were performed to examine the key gene and protein expressions of the Wnt/β-catenin signaling pathway. BMSCs were cocultured with the different membranes for 12, 24, 48, and 72 h, respectively. The qPCR analysis revealed that the expression levels of the essential genes (eg, *AXIN1, AXIN2, β-catenin, LRP5, LRP6, GSK3β*, and *WNT3A*) involved in the Wnt/β-catenin pathway in BMSCs were significantly higher in the PSGC membrane than in the control group and PG membranes after 24 and 72 h of coculturing with BMSCs. Furthermore, the expression levels of *AXIN2, β-catenin, LRP5, LRP6*, and *GSK3β* increased in the PSGC membrane after 12 h. In addition, compared with the control group and PG membranes, *β-catenin* and *LRP6* expression levels significantly increased in the PSGC membrane after 48 h of coculture (Figure 5a–g). Figure 4e shows the Western blot results, where *β-catenin* and *WNT3A* protein expression levels in the BMSCs cocultured for 7 days with the PSGC membranes were significantly enhanced compared

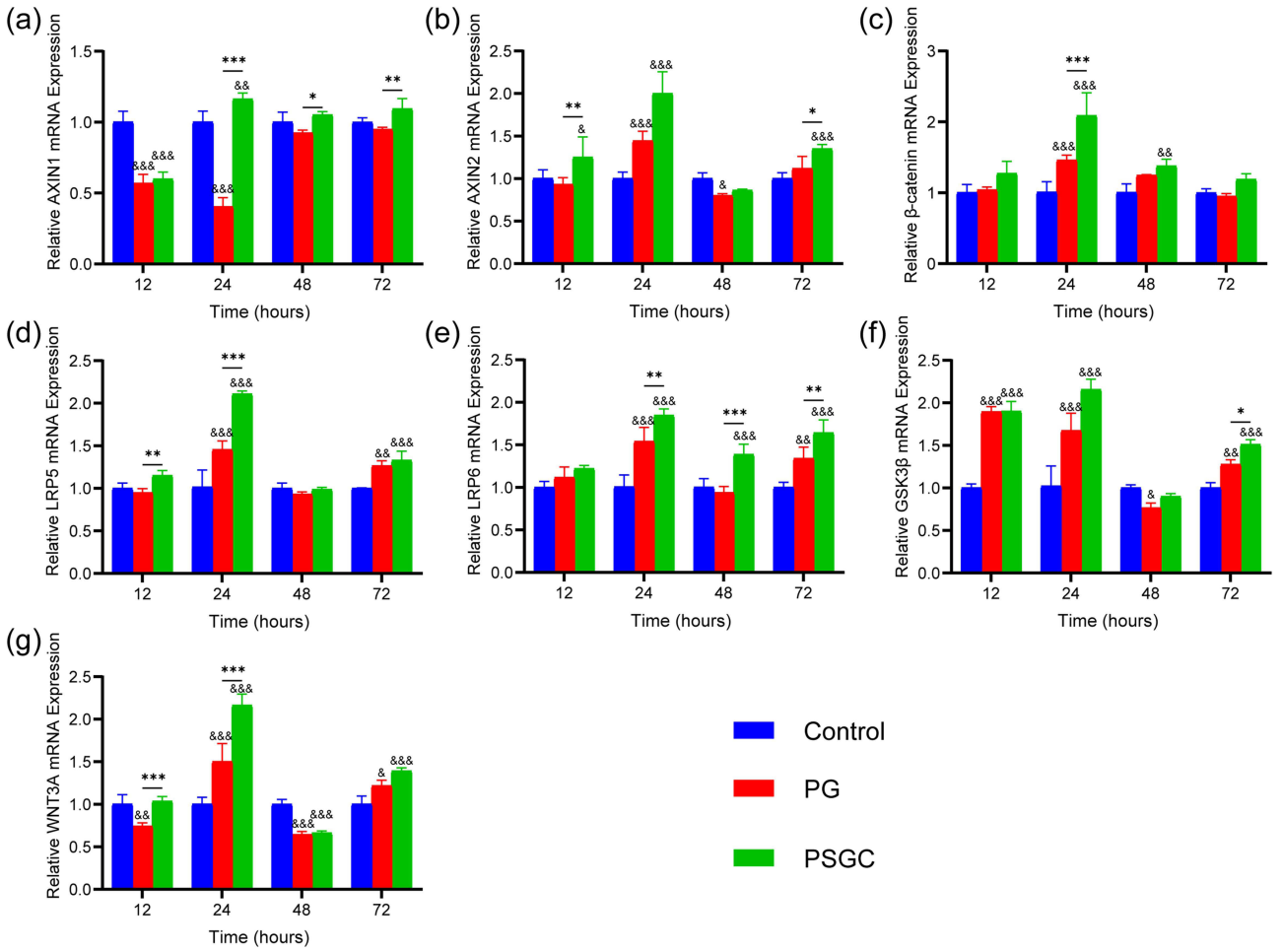

Figure 5 SAL- and CT-loaded nanofiber membranes activate the Wnt/β-catenin pathway. (**a–g**) Wnt/β-catenin pathway–associated gene expression after coculturing BMSCs with different nanofiber membranes for 0.5, 1, 2, and 3 days. Results are expressed as the mean ± standard deviation (n = 3). $^{\&}p < 0.05$, $^{\&\&}p < 0.01$, and $^{\&\&\&}p < 0.001$. $^{*}p < 0.05$, $^{**}p < 0.01$, and $^{***}p < 0.001$.

with those in the BMSCs cocultured with the control group and PG membranes (Figure 4e, h and i). These findings demonstrate that the drug release from the PSGC membranes could activate the Wnt/β-catenin signaling pathway.

SAL- and CT-Loaded Nanofiber Membranes Synergistically Promote BMSC Differentiation Through the Wnt/β-Catenin Signaling Pathway

To further verify the osteogenic activity of the PSGC membranes, the Wnt/β-catenin signaling pathway promotes osteogenesis. DKK-1 was used to assess the role of the Wnt/β-catenin signaling pathway in BMSC differentiation. qPCR results revealed that in the PSGC membrane, *LRP6* and β-catenin expression levels were significantly downregulated when the Wnt/β-catenin pathway was blocked using DKK-1. Furthermore, *RUNX2* and *OCN* expression levels, which are osteogenesis-

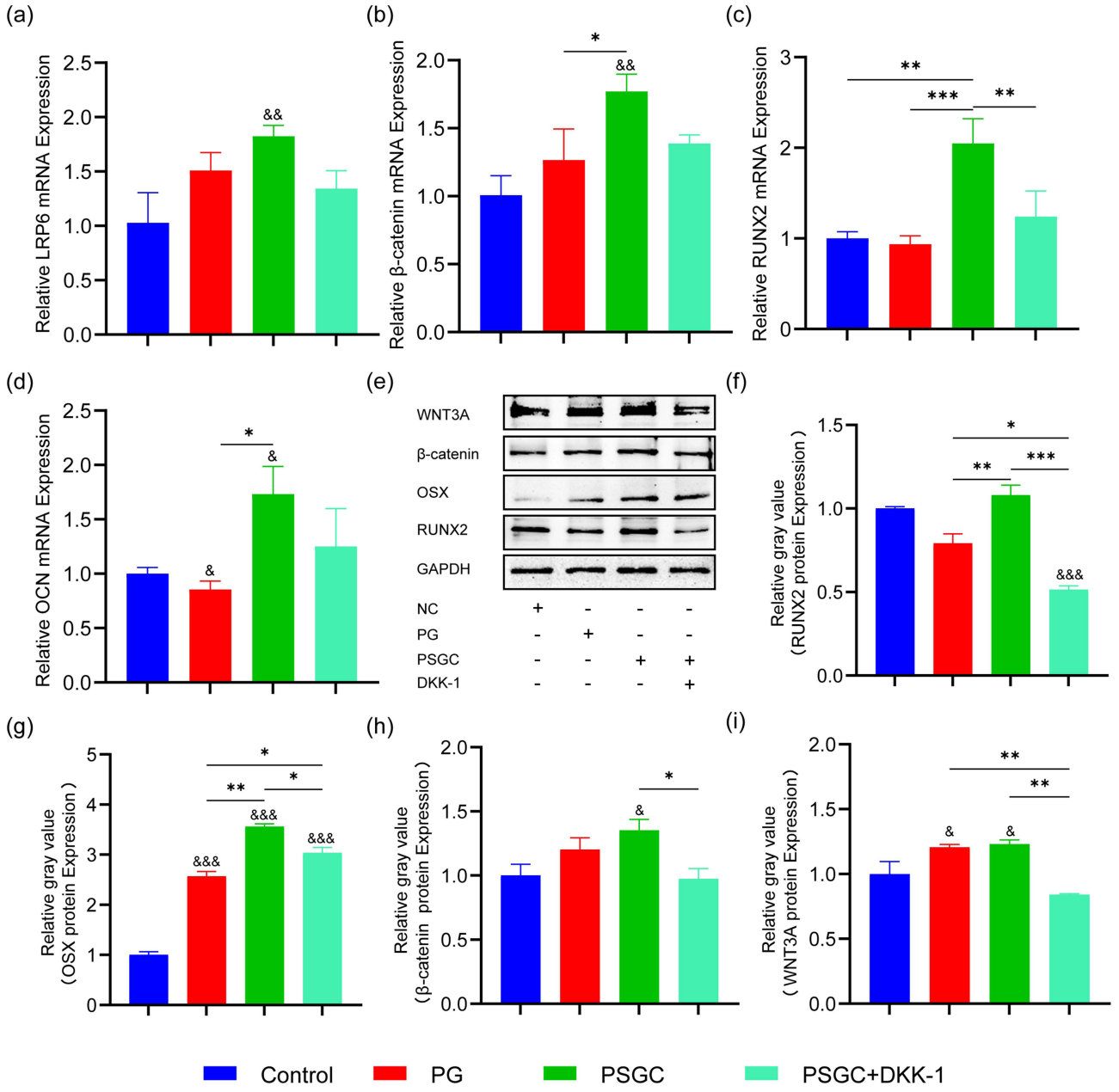

Figure 6 SAL and CT-loaded nanofiber membranes synergistically promote BMSC differentiation through the Wnt/β-catenin signaling pathway. (**a**–**d**) The expression of key genes of the Wnt/β-catenin pathway and the osteogenic marker gene at 24 h. (**e**) Western blot results after BMSCs were cocultured with the different membranes for 24 h. Results are expressed as the mean ± standard deviation (n = 3). (**f**–**i**) Quantitative analysis of Western blot results from (**e**). $^{\&}p < 0.05$, $^{\&\&}p < 0.01$, and $^{\&\&\&}p < 0.001$. $^{*}p < 0.05$, $^{**}p < 0.01$, and $^{***}p < 0.001$.

related marker genes, decreased when treated with DKK-1 in the PSGC membranes cocultured with BMSCs compared with those in PSGC membranes cocultured with BMSCs without DKK-1 treatment (Figure 6a–d). The Western blot results revealed that *WNT3A, β-catenin, OSX*, and *RUNX2* protein expression levels were significantly reduced in the PSGC membranes when the Wnt/β-catenin pathway was inhibited using DKK-1 (Figure 6e–i). Our data suggest that the Wnt/β-catenin signaling pathway participates in osteogenic differentiation in the PSGC membrane when cocultured with BMSCs.

Assessment of Biocompatibility of HUVECs on the Coaxial Electrospun Nanofiber Membranes

To evaluate the biocompatibility of HUVECs with the different membranes, live/dead cell staining was performed. Figure 7a shows the results of live/dead cells. A larger number of live cells (green) were found in the different membranes that were cocultured with HUVECs. In contrast, only a very small number of dead cells (red) were seen in different membranes. These findings are consistent with the results of coculturing BMSCs with the membranes.

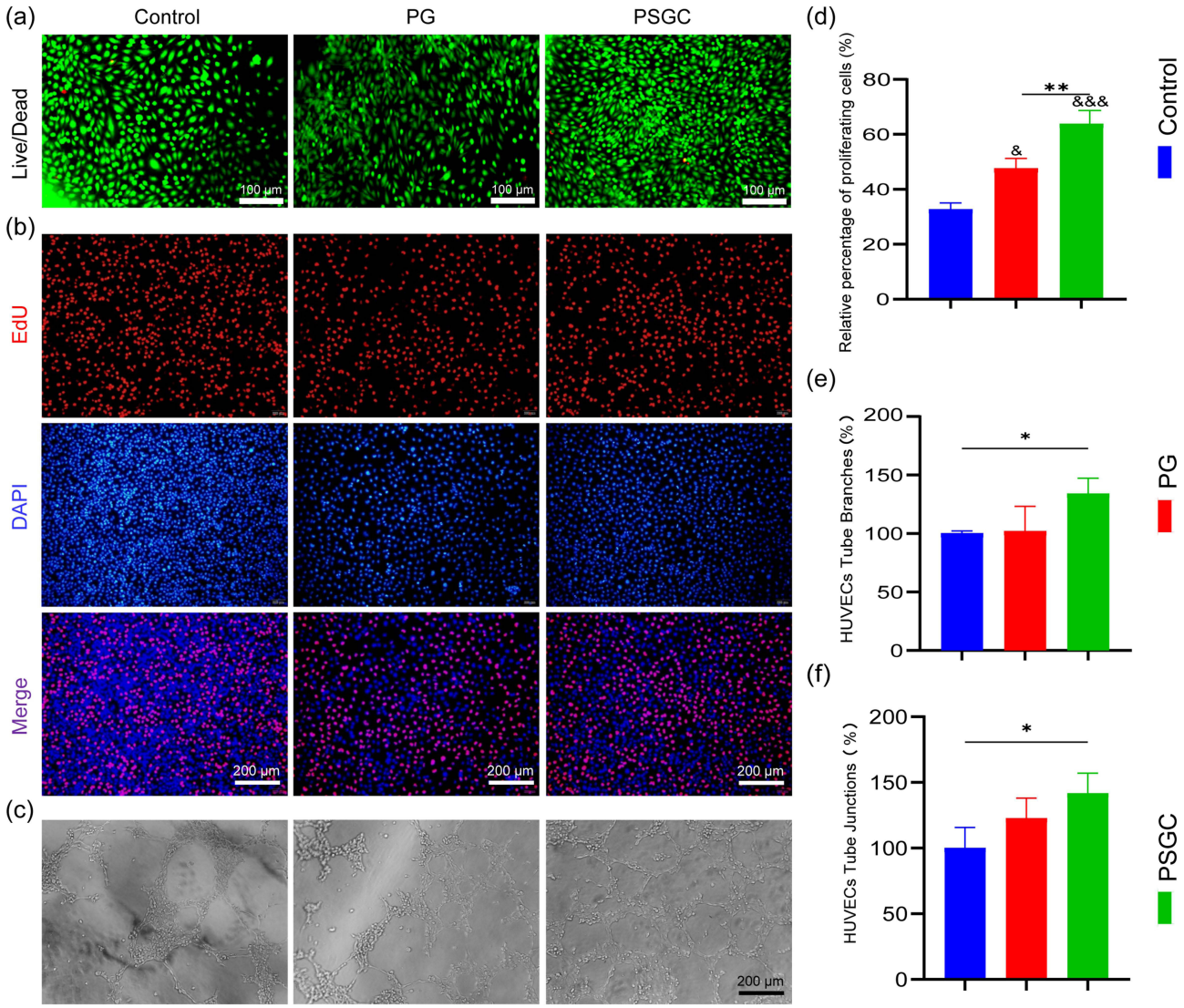

Figure 7 Biocompatibility and angiogenic ability evaluation of HUVECs cocultured with the different nanofiber membranes. (**a**) Live/dead cell straining for HUVECs incubated together with different nanofiber membranes on day 3. Red and green indicate dead and living cells, respectively. (**b**) The proliferation ability of HUVECs cocultured with PG and PSGC nanofiber membranes was reflected by the EdU assay. (**c**) Tube structure-building experiments with HUVECs. (**d**) The numerical evaluation of EdU outcomes. (**e** and **f**) Quantitative analysis of tube branches and junctions in tube formation. Results are expressed as the mean ± standard deviation (n = 3). $^{\&}p < 0.05$, and $^{\&\&\&}p < 0.001$. $^{*}p < 0.05$, $^{**}p < 0.01$.

Abbreviations: HUVECs, human umbilical vein endothelial cells; PG, PCL/Gelatin; PSGC, PCL/SAL /Gelatin/CT; EdU, 5-Ethynyl-2'-deoxyuridine.

The EdU assay was used to evaluate the cell proliferation of HUVECs cocultured with different membranes. The rate of cells proliferating was 32.66% ± 1.92% (control group), 47.48% ± 3.73% (PG membrane), 63.71% ± 5.52% (PSGC membrane), which was considerably increased in the PSGC membrane compared to the control group and PG membranes (Figure 7b and d). This assay proved the minimal toxicity and high biocompatibility of the coaxial electrospun membranes.

Tube Formation Ability

The HUVEC tube formation experiment demonstrated that the PSGC membranes exhibited the best tube formation ability compared with the control group and PG membranes. Furthermore, the tube formation ability was better in the PG membrane than in the control group (Figure 7c). The quantitative analysis of tube formation showed that the junction and tube branching numbers were higher in the PSGC than those of the control group and PG membranes (Figure 7e and f), indicating its superior tube formation ability.

Vascularization Ability of the Electrospun Nanofiber Membranes

To further prove the vascularization capacity of the different membranes, qPCR was performed to analyze the expression levels of the vascularization-related marker genes, including those of *CD31, PDGF*, and *NOS3*. On days 1 and 3, the expression levels of *CD31, PDGF*, and *NOS3* in the HUVECs cocultured with the PSGC membrane were notably increased compared with those in the HUVECs cocultured with the control group and PG membranes (Figure 8a). Figure 8b shows the immunofluorescence labeling of CD31 protein in HUVECs. Comparing the PSGC membrane to the control group and PG membranes, CD31 protein expression was significantly higher in the former, consistent with the results of the quantitative analysis (Figure 8c). VEGF plays an important role in vascularization. Herein, the ELISA results revealed that the levels of VEGF protein in the cocultured supernatants of HUVECs cocultured with the PSGC membrane were significantly higher compared with those in the HUVECs cocultured with the control group and PG membranes (Figure 8d). The expression levels of CD31 and VEGF in each group were verified using Western blot analysis, which revealed that their expression levels were elevated in the PSGC membrane compared with those in the control group and PG membranes (Figure 8e–g). Therefore, the PSGC membrane possesses the capacity to induce HUVEC vascularization.

Microcomputed Tomography

At 8 weeks after surgery, we used microcomputed tomography (micro-CT) to rebuild the tissue of the rat cranial defect. Only a small amount of new bone regenerated from the edge of the defect in the control group (Figure 9). Furthermore, only a small amount of newly formed bone in the middle of the defect could be seen in the PG and PGS membranes. The PGC group showed a larger amount of the newly formed bone in the middle of the defect at 8 weeks after the surgery. Conversely, in the PSGC membrane, the defect was almost completely covered by the newly formed bone (Figure 9a). According to the quantitative analysis of micro-CT, the PSGC membranes exhibited significantly higher values of BV (14.81 ± 1.89), BV/TV (36.97 ± 4.71), and trabecular number (1.29 ± 0.24) than the other membranes (Figure 9b–d), suggesting that the PSGC membranes could boost cranial bone regeneration in rats.

Histological Analysis

To assess bone regeneration, we used H&E and Masson′s trichrome staining. At 8 weeks post-surgery, the control and PG groups exhibited a greater number of connective tissues in the bone defect area, but only a smaller new bone was created at the defect's margin. In addition, more newly formed bone in the middle of the bone defect area was noted in the PSG and PGC groups. However, in the PSGC group, a larger amount of new bone formation was observed in the middle of the bone defect area (Figure 10a). Masson′s staining images after 8 weeks of surgery revealed that in the PSGC group, a considerable amount of new bone collagen was deposited at the center of the bone defect area. Furthermore, more new bone formation and collagen deposition were observed in the PSG and PGC groups (Figure 10b). Further quantitative analysis of these staining methods showed that the PSGC group had much more new bone growth and deposition than the other groups (Figure 10c and d), indicating the PSGC membrane was superior to the other membranes for bone regeneration.

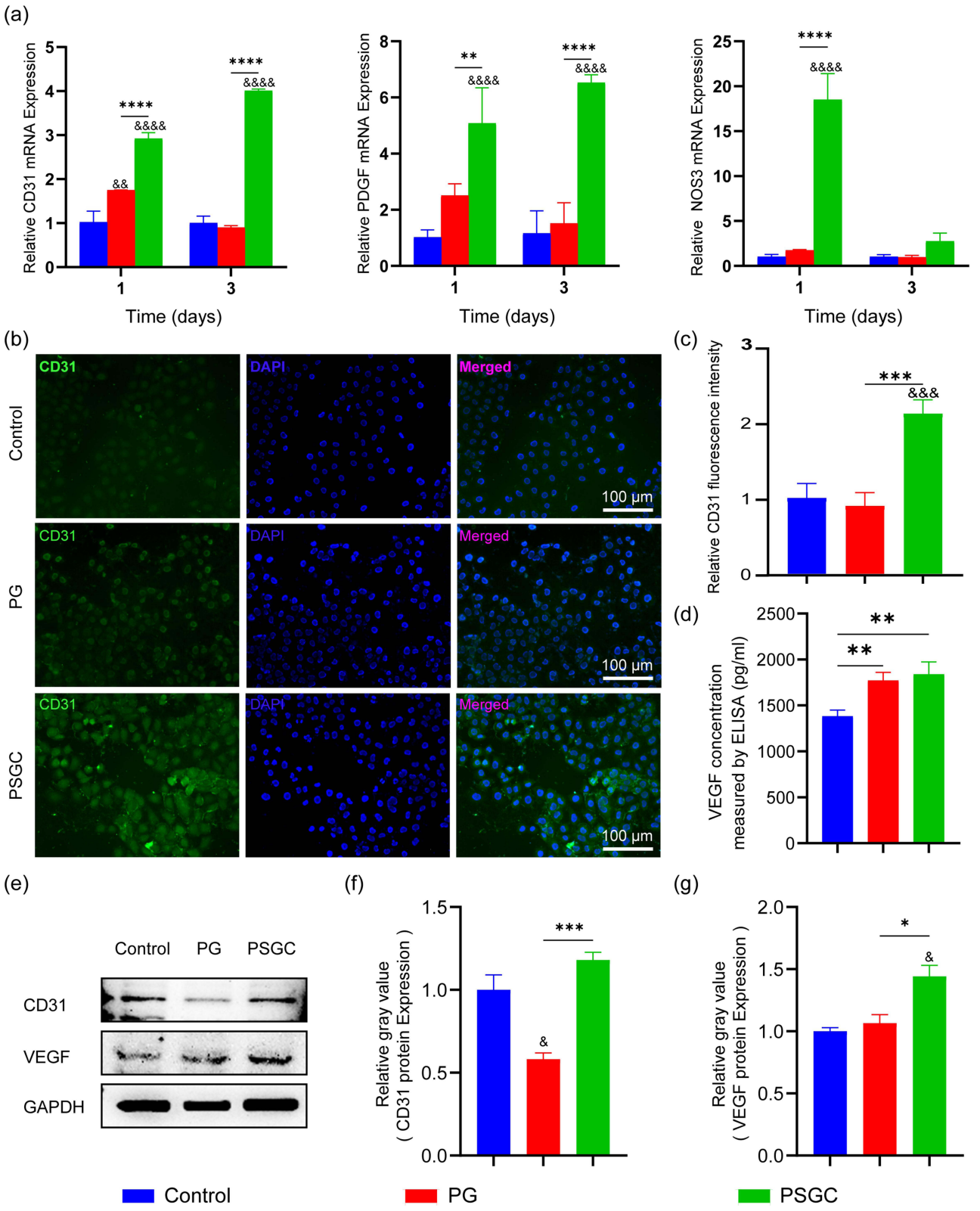

Figure 8 In vitro vascularization evaluation of HUVECs cocultured with different nanofiber membranes. (**a**) *CD31*, *PDGF*, and *NOS3* mRNA expression on days 1 and 3. (**b**) Representative images of the CD31 immunofluorescence assay of HUVECs cocultured with different nanofiber membranes for 3 days. (**c**) Quantitative analyses of CD31 protein from (**b**). (**d**) ELISA assay to detect the concentration of VEGF secreted by HUVECs. (**e**) The results of CD31 and VEGF protein expression levels in different nanofiber membranes on day 3. (**f** and **g**) Quantitative analyses of CD31 and VEGF protein expression from (**e**). Results are expressed as the mean ± standard deviation (n = 3). $^{\&}p < 0.05$, $^{\&\&}p < 0.01$, $^{\&\&\&}p < 0.001$, and $^{\&\&\&\&}p < 0.0001$. $^{*}p < 0.05$, $^{**}p < 0.01$, $^{***}p < 0.001$, and $^{****}p < 0.0001$.

Abbreviations: CD31, platelet endothelial cell adhesion molecule-1; PDGF, platelet derived growth factor; NOS3, recombinant nitric oxide synthase 3; ELISA, enzyme-linked immunosorbent assay.

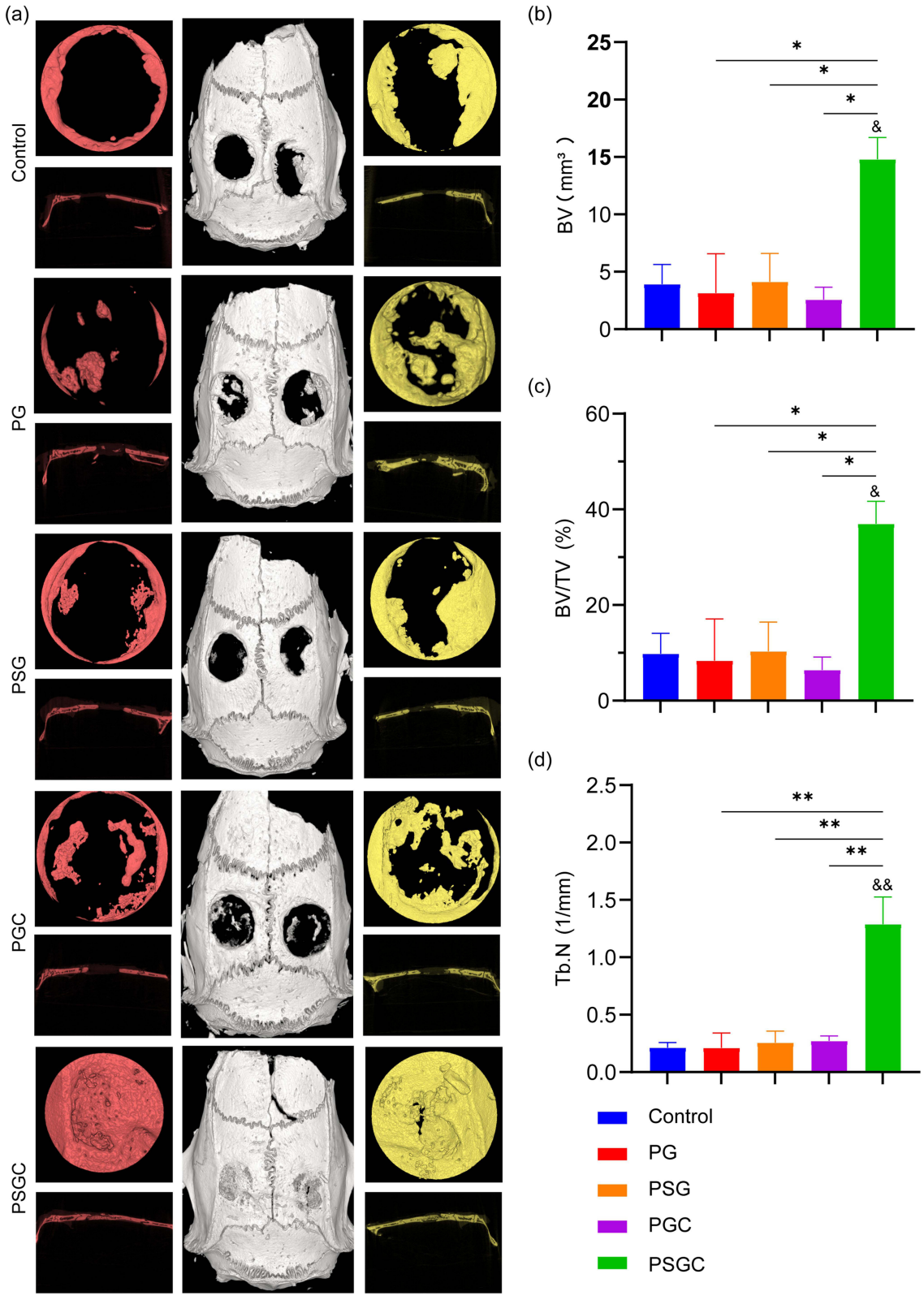

Figure 9 Micro-CT scanning and analysis. (**a**) Micro-CT imaging of the different groups after 8 weeks of surgery. Within the 5-mm-diameter circle, the freshly created bone tissue is indicated in red and yellow. (**b**) Bone volume. (**c**) BV/TV. (**d**) Tb.N. Results are expressed as the mean ± standard deviation (n = 3). $^{\&}p < 0.05$ and $^{\&\&}p < 0.01$. $^{*}p < 0.05$ and $^{**}p < 0.01$.

Abbreviations: BV/TV, bone volume fraction; Tb.N, trabecular bone number.

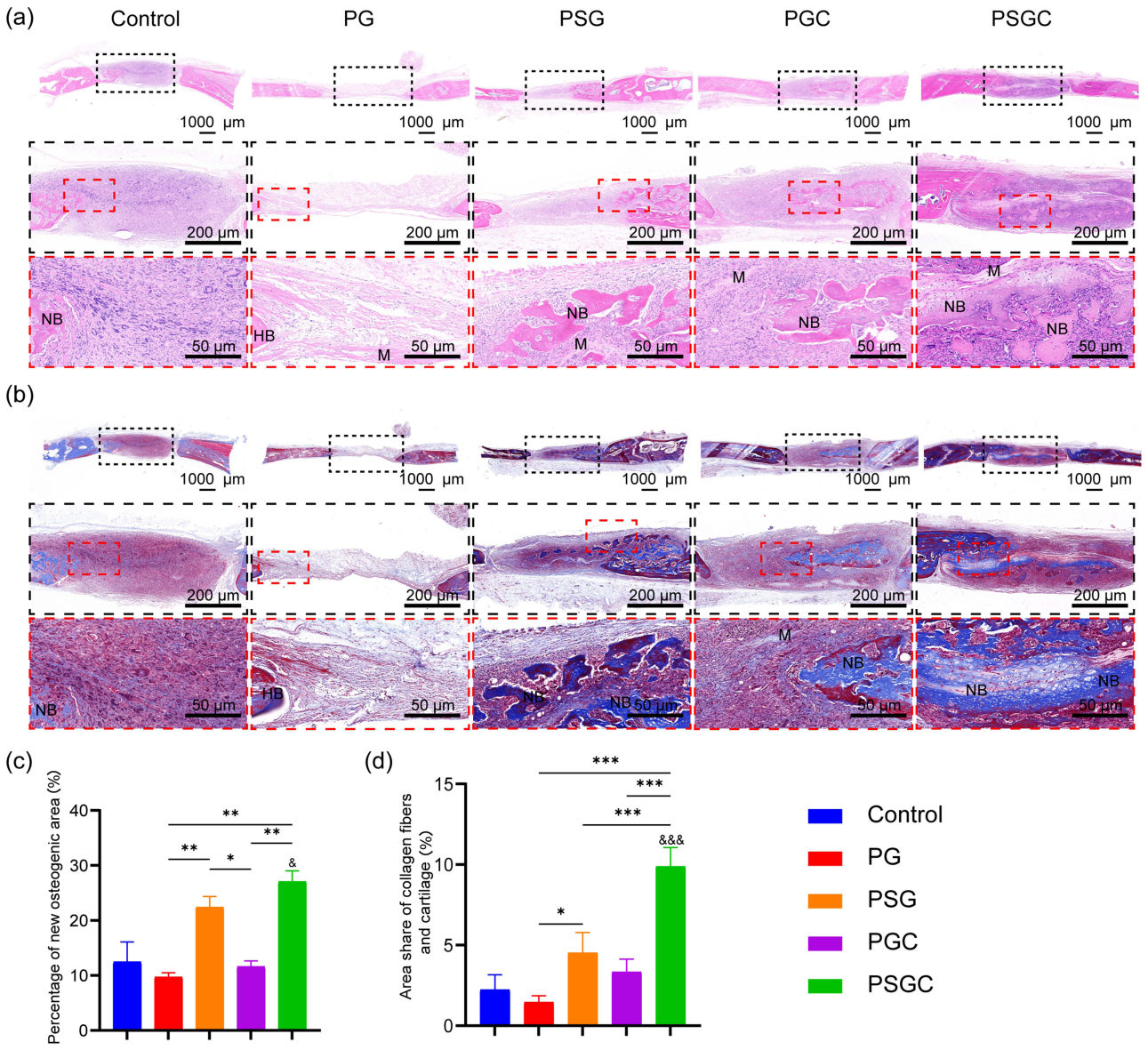

Figure 10 Results of H&E and Masson's trichrome staining for different membranes in the rat skull tissue model 8 weeks after surgery. (**a**) H&E staining. (**b**) Masson's staining. The selected expanded region is shown by black and red boxes. NB: new bone; HB: host bone: (M) materials. (**c**) Quantitative analyses of the percentage of new bone from (**a**). (**d**) Quantitative analyses of the percentage of collagen deposition from (**b**). Results are expressed as the mean ± standard deviation (n = 3). $^{\&}p < 0.05$, and $^{\&\&\&}p < 0.001$. $^{*}p < 0.05$, $^{**}p < 0.01$, and $^{***}p < 0.001$.

Immunohistochemistry

To further verify the osteogenic ability of the PSGC membrane, Immunohistochemistry was conducted to assess the osteogenesis-related protein expression in the bone defect area at 8 weeks post-surgery. In the control and PG groups, there were a few OSX, RUNX2, COL1, and OCN-positive areas at the edge of the defect (Figure 11a–d). However, in the PSGC groups, a significant increase was found in the middle of the bone area. Further quantitative analysis showed that, in the PSGC groups, OSX, RUNX2, COL1, and OCN proteins exhibited higher expression than those of the other group (Figure 11e–h). Hence, given these results, we demonstrated that the PSGC membrane via drug release increased osteogenesis-related protein expression and bone regeneration, which are consistent with the results of micro-CT, H&E, and Masson′s trichrome staining methods.

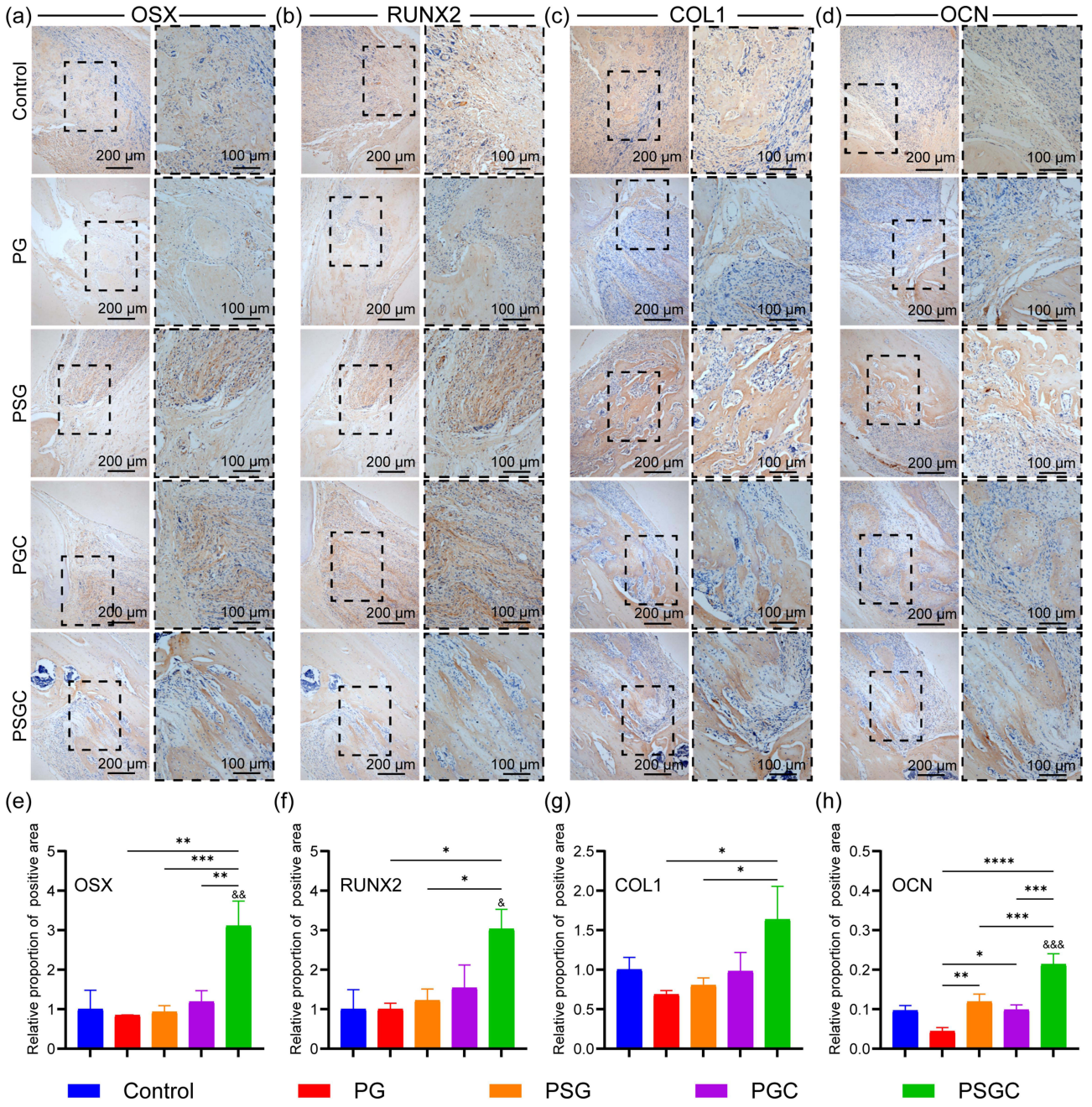

Figure 11 At 8 weeks after surgery, immunohistochemistry findings for several membranes in a rat cranium defect model. (**a**) OSX. (**b**) RUNX2. (**c**) COL1. (**d**) OCN. (**e–h**) Quantitative analyses of positive OSX, RUNX2, COL1, and OCN proteins from (**a–c**), and (**d**) in different groups. Results are expressed as the mean ± standard deviation (n = 3). $^{\&}p < 0.05$, $^{\&\&}p < 0.01$, and $^{\&\&\&}p < 0.001$. $^{*}p < 0.05$, $^{**}p < 0.01$, $^{***}p < 0.001$, and $^{****}p < 0.0001$.

Abbreviations: OSX, osterix; RUNX2, runt-related transcription factor 2; COL1, collagen I; OCN, osteonectin.

In vivo Evaluation of Vascularization in the Subcutaneous Layer of Rats

We confirmed that the PSGC membrane could induce HUVEC vascularization. To further verify the vascularization ability, different membranes were implanted onto the subcutaneous area of rats for 2 and 4 weeks. At 2 weeks post-implantation in the PG membrane, only a few blood vessels were detected at the edge and on the surface of the membrane. The number of blood vessels in the PSG and PGC membranes was more as compared with that in the PG membrane. Conversely, the PSGC membrane showed a larger number of newly formed blood vessels at the edge and on the surface of the membrane than the remaining groups (Figure 12a). The H&E staining results are shown in Figure 12b

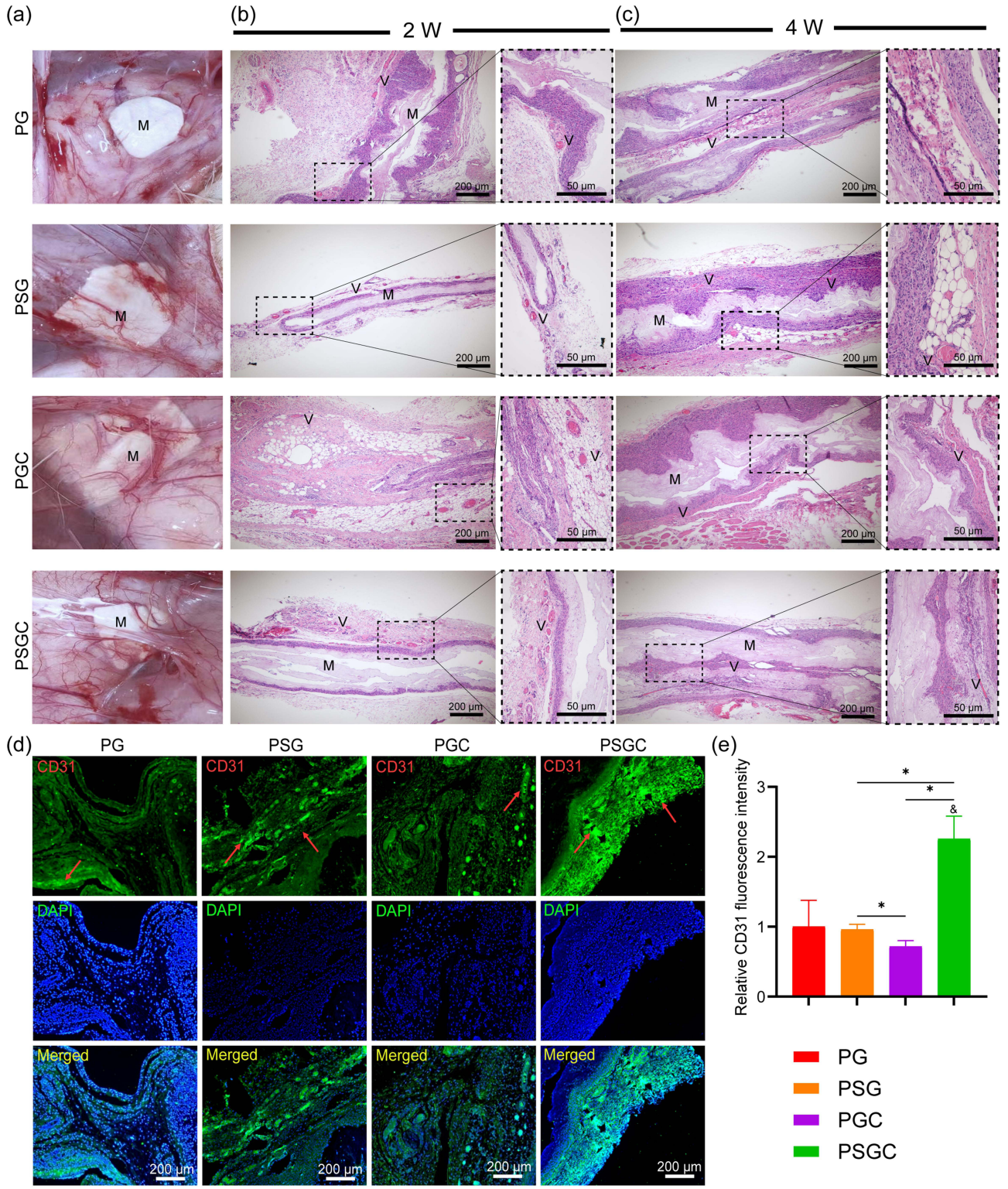

Figure 12 Evaluation of the vascularization effect of different membranes in vivo at 2 and 4 weeks. (**a**) Figure of a nanofiber membrane placed subcutaneously in rats for 2 weeks. (**b**) Representative H&E staining images of different membranes implanted in rats subcutaneously for 2 weeks. (**c**) Representative H&E staining images of different membranes implanted in rats subcutaneously for 4 weeks. (**d**) CD31 immunofluorescence images; arrows represent CD31. (**e**) Quantitative analysis of the CD31 expression from (**d**). (M) material; (V) blood vessel. Results are expressed as the mean ± standard deviation (n = 3). $^{\&}p < 0.05$ and $^{*}p < 0.05$.
Abbreviations: H&E, histologically stained via hematoxylin and eosin; CD31, platelet endothelial cell adhesion molecule-1.

and c. At 2 weeks post-implantation, the number of blood vessels were significantly increased in the PSGC membrane compared with that in the other membranes. By 4 weeks post-implantation, compared with the PG, PSG, and PGC membranes, the number of blood vessels in the PSGC membrane had significantly increased. Thus, the PSGC membrane exhibited abundance formation of new blood vessels in the middle (Figure 12b and c).

To better analyze the vascularization, tissue slices were collected at 2-weeks post-implantation. The CD31 protein, a neovascularization marker protein, was detected using immunofluorescence. In the PSGC membrane, the fluorescence intensity (green) was considerably higher than that in the other membranes. In addition, a larger number of CD31-positive cells was observed in the PSGC membrane compared with that in the other membranes (Figure 12d). Further quantitative analysis revealed that the CD31 protein expression in the PSGC membrane was significantly high than that in the other membranes (Figure 12e). Our results indicate that the PSGC membrane exhibits good vascularization ability.

In vivo Vascularization Assessment in Rat Cranial Bones

Figure 13 depicts the CD31 and VEGF immunofluorescence staining images of the graft implanted in rat cranial bones at 8 weeks post-operation. Figure 13a shows the CD31 expression level, in which the PSGC membrane exhibited much higher fluorescence intensity (red) compared with the PG, PSG, and PGC membranes, thus indicating higher expression of CD31 in the PSGC membrane and a larger number of fresh blood vessel formations in the bone defect. Figure 13b depicts the VEGF expression images of the graft implanted in rat cranial bones at 8 weeks post-operation. Compared with the PG, PSG, and PGC membranes, VEGF expression in the PSGC membrane was also enhanced in the bone defect. These results revealed that higher expression of CD31 and VEGF in the PSGC membrane contributes to new blood vessel formation and bone regeneration.

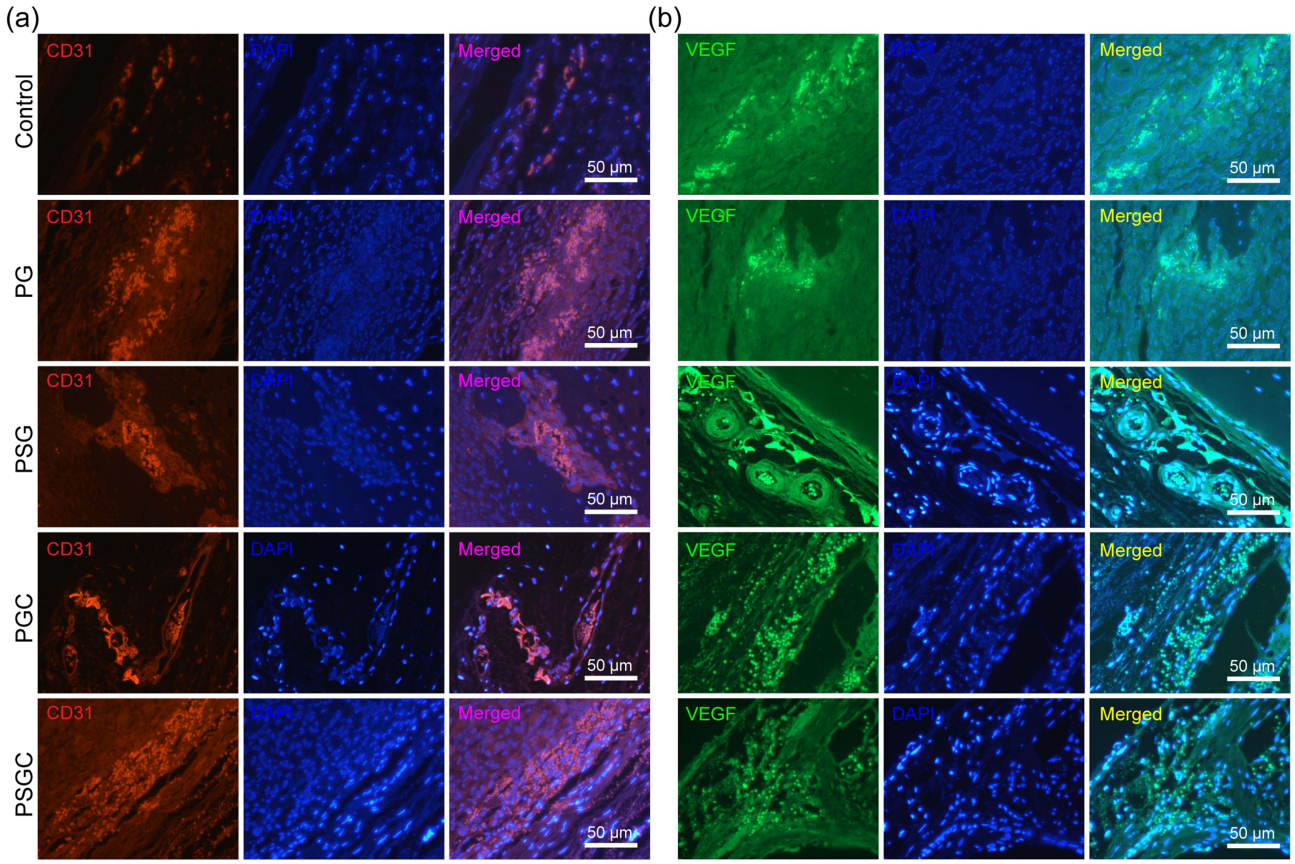

Figure 13 Images of rat skull slices subjected to immunofluorescence at 8 weeks post-surgery. (**a**) CD31. (**b**) VEGF. Red fluorescence represents the CD31 protein and green fluorescence represents the VEGF protein. Bar = 50 μm.
Abbreviations: CD31, platelet endothelial cell adhesion molecule-1; VEGF, vascular endothelial growth factor.

Discussion

Bone anomalies, a prevalent orthopedic condition, involve long treatment durations and cause considerable harm to organisms, and thus, remain one of the key obstacles in clinical practice. Thus, developing novel biomimetic artificial bone repair materials that can replicate the composition and structural features of natural bone has become one of the primary trends for the treatment of such conditions. Electrospun nanofibers are commonly used in bone tissue engineering. For instance, coaxial electrospun nanofiber membranes are used for administering drugs owing to their unique core–shell structure. Herein. We used coaxial electrostatic spinning technology to develop a dual drug–release system containing SAL and CT that can be controlled locally. This novel drug-delivery technology demonstrated a dual effect of stimulating osteogenesis and vascularization at localized deficiencies. Furthermore, the PSGC membranes exhibited the most successful osteogenic activity in a bone-deficient animal model.

The coaxial electrospun nanofiber membranes were evaluated to confirm the presence and effect of each polymer used. In terms of shape, fluorescent microscopy images confirmed the structural integrity of the gelatin shell and the PCL core layer of the membranes. PCL can provide adequate support to the membrane, compensating for the inferior mechanical qualities of gelatin; however, gelatin has a high bioaffinity, which promotes adhesion between the nanofiber membrane and the wound exudate during premedication. Furthermore, the nanofiber membrane exhibits excellent porosity, permeability, and water absorption, which can improve gas exchange and enable nutrient intake and metabolic waste exchange, consequently boosting angiogenesis and bone repair. In the experiment conducted to determine the membrane biodegradation rate, the nanofiber membrane rapidly degraded initially and then gradually slowed down. This is because the exterior layer of the membrane is gelatin, a large hydrophilic molecule that is insoluble in water but absorbs 5–10 times more water when immersed in it, swells and softens, and dissolves into a gel when heated. The gelatin portion of the shell layer dissolves into the gel in a PBS environment at 37 °C, with the membrane biodegradation rate becoming the highest in 5 days. A high biodegradation rate aids biomaterial metabolism and utilization in vivo.

In the PSGC membrane, SAL and CT are encapsulated in the core and shell layers of the nanofiber membrane, respectively. Previous studies have reported that collagen not only exhibits greater elasticity than skin but also promotes connective tissue repair.[40] Hydrolyzed collagen supplements (such as gelatin) can alleviate joint pain and increase cartilage density, making joints more durable. When the material is implanted into the body after skeletal trauma, the dissolution of gelatin is accompanied by the rapid local release of drugs, allowing the material to adhere well to the implantation site while CT infiltrates the wound along with gelatin. Therefore, in the early stage of material implantation, CT molecules and gelatin provide a large amount of favorable factors for bone tissue repair. The release of SAL stabilized on the 14th day after implantation and continues thereafter, thereby meeting the expected requirements for long-term sustained drug release. The slower release rate of SAL compared with that of CT is due to the hydrophobic nature of PCL,[41,42] which partially encapsulates the drugs within its structure, slowing down their diffusion in the medium. Owing to the presence of the gelatin shell structure, the entire core layer is wrapped inside, prolonging the diffusion path of the inner-layer drugs into the medium, thereby achieving a slower drug release and successful drug release control. However, during the electrospinning process, some drugs still migrate to the nanofiber surface, leading to sudden release during the prerelease stage (~18% drug released within 12 h), which is a disadvantage of coaxial electrospinning. Thus, CT is released from the coaxial nanofiber shell in a combined mode of diffusion- and degradation-based release, while SAL in the core mainly relies on PCL biodegradation for release.

In vitro cell experiments revealed that the SAL–CT corelease system exhibits good osteogenic effects on BMSCs while promoting angiogenesis in HUVECs. This further confirms the coupling relationship between bone and blood vessel formation, consistent with the findings of Kumar et al and Lafage-Proust et al[43,44] On the first day of co-culture of BMSCs and cells in each group during the CCK-8 assay experiment, there were no significant differences in the OD values at 450 nm. On the 3rd day, the OD values of the PG and PSGC groups were slightly lower than those of the control group. This can be attributed to the degradation of scaffolds and release of drugs in these two groups, which exerted some initial stimulation and influence on the cells. However, this minor influence appeared to stabilize by the 5th day, as there were no significant differences in the OD values between the groups. The CCK-8 assay revealed that BMSCs proliferated with increasing time, thereby verifying the importance of the early promotion of BMSC recruitment for osteogenesis, consistent with the findings of Mu et al.[45] The gradual increase in OD values observed from day 1

to day 5 in the CCK-8 detection experiment indicates a progressive proliferation of cells and an overall increase in cell numbers. Herein, we believe that the chief action mechanism underlying the PSGC membrane fabricated using coaxial electrospinning is the abundant provision of favorable factors by CT and gelatin during the early stage, while SAL promotes osteogenesis and angiogenesis coupling throughout the repair process, encouraging osteogenic differentiation via the Wnt/β-catenin pathway. In a previous study, Guo et al demonstrated that SAL can improve angiogenesis–osteogenesis coupling by regulating the HIF-1α/VEGF signaling pathway.[46] Furthermore, Li et al reported that SAL enhanced the expression of WNT3A and β-catenin through the Wnt/β-catenin signaling pathway, promoting osteogenic differentiation.[26] Thus, extensive cell experiments were conducted to validate these findings and hypotheses. The qPCR and Western blotting results were consistent, as anticipated, showing elevated expression levels of WNT3A and β-catenin in the PSGC membrane. The addition of DKK-1 significantly downregulated the related genes and proteins compared with that in the absence of DKK-1 addition in the PSGC membrane, further indicating that PSGC scaffolds promote the expression of osteogenic-related genes through the Wnt/β-catenin signaling pathway. The qPCR results revealed that the expression levels of certain osteogenic and angiogenic factors in BMSCs and HUVECs did not increase with time. This is because there are many factors influencing gene expression when comparing genes along the time axis, among which a crucial factor is that the expression of many genes change with time. However, regardless of the time period, the PSGC membrane showed superior results compared with those of the control group and unloaded drug groups. VEGF and CD31 are markers of early angiogenesis.[47,48] This study further validated the early promotion of angiogenesis by the SAL–CT dual drug–delivery system at the gene and protein levels.

In a study involving the nanofiber membranes implanted in rat cranial bone defects, our results revealed that the PSGC membrane exhibited better results in terms of osteogenesis and angiogenesis compared with those in the control group, PSG,

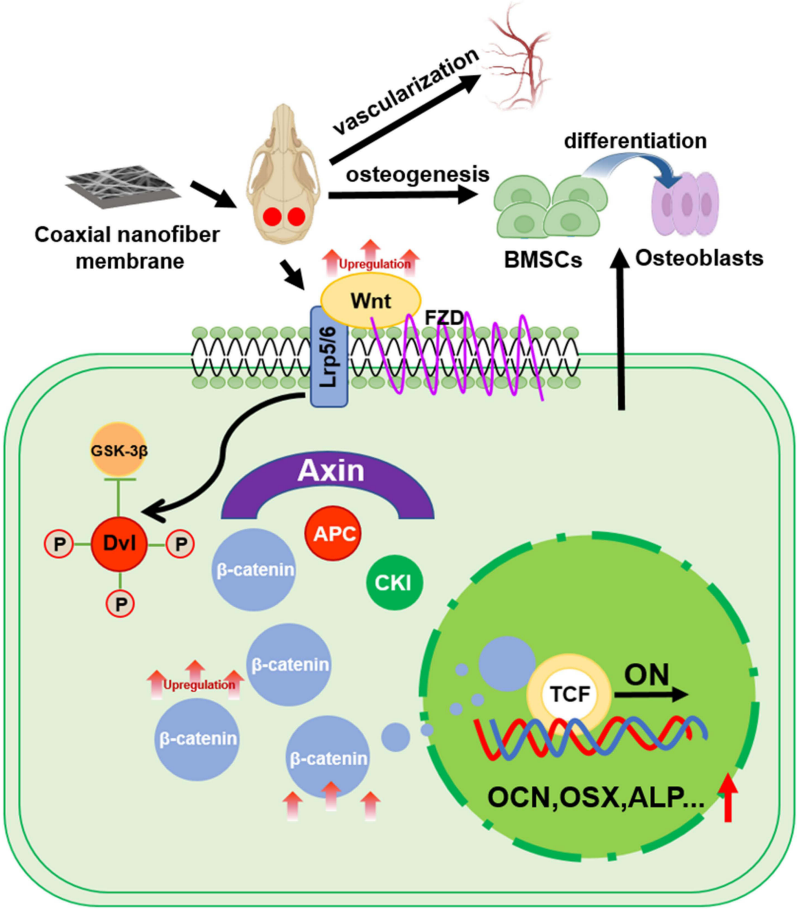

Figure 14 Diagram of the mechanism by which PSGC nanofiber membranes promoting osteogenesis and vascularization.
Abbreviation: FZD, frizzled; OCN, osteonectin; OSX, osterix; RUNX2, runt-related transcription factor 2.

and PGC membranes. Additionally, the PSGC membrane outperformed the other membranes loaded with only one drug in terms of the osteogenesis and vascularization effects. This was primarily because of the following reasons: (1) CT was effective when the material was implanted in rats alongside partially degraded gelatin, exhibiting a high bioaffinity and allowing the attachment of the nanofiber membrane to the wound exudate. (2) SAL worked locally alongside PCL biodegradation, stimulating the Wnt/β-catenin pathway and boosting the expression of osteogenesis-related proteins and genes. Furthermore, SAL continues to play a role in PSGC implantation. (3) The synergistic effects of SAL and CT play a key role in coupling angiogenesis and bone regeneration. Thus, the PSGC membranes exhibited excellent osteogenesis capacity.

Conclusion

Herein, we fabricated nanofiber membranes using the coaxial electrospinning technique and found that the PSGC membranes loaded with SAL and CT were superior in promoting angiogenesis and bone repair and exhibited good biocompatibility compared with the other membranes. The coaxial structure of the nanofiber membranes allowed for long-term, spatially targeted drug release. The PSGC membrane released drugs by activating the Wnt/β-catenin pathway, which enhanced osteogenic gene expression and promoted osteogenesis (Figure 14). Thus, the controlled release of SAL and CT accompanied by the release of gelatin degradation in PSGC membranes promoted bone repair and angiogenesis of bone defects in rats. Therefore, this novel membrane is an excellent material for bone healing.

Acknowledgments

This study has been financed by Clinical Research Project of Changzhou Medical Center of Nanjing Medical University (CMCB202206), and the Key Project of Science and Technology of Jiangsu Province (BE2018644).

Disclosure

The authors report no conflicts of interest in this work.

References

1. Schmidt AH. Autologous bone graft: is it still the gold standard? *Injury*. 2021;52:S18–S22. doi:10.1016/j.injury.2021.01.043
2. Dimitriou R, Jones E, McGonagle D, et al. Bone regeneration: current concepts and future directions. *BMC Med*. 2011;9(1):66–75. doi:10.1186/1741-7015-9-66
3. Bauer TW, Muschler GF. Bone graft materials. An overview of the basic science. *Clin Orthop Relat Res*. 2000;10(371):10–27.
4. Ye K, Kuang H, You Z, et al. Electrospun nanofibers for tissue engineering with drug loading and release. *Pharmaceutics*. 2019;11(4):182. doi:10.3390/pharmaceutics11040182
5. Lin WH, Yu J, Chen G, et al. Fabrication of multi-biofunctional gelatin-based electrospun fibrous scaffolds for enhancement of osteogenesis of mesenchymal stem cells. *Colloids Surf B Biointerfaces*. 2016;138:26–31. doi:10.1016/j.colsurfb.2015.11.017
6. Li C, Vepari C, Jin HJ, et al. Electrospun silk-BMP-2 scaffolds for bone tissue engineering. *Biomaterials*. 2006;27(16):3115–3124. doi:10.1016/j.biomaterials.2006.01.022
7. Martins A, Duarte AR, Faria S, et al. Osteogenic induction of hBMSCs by electrospun scaffolds with dexamethasone release functionality. *Biomaterials*. 2010;31(22):5875–5885. doi:10.1016/j.biomaterials.2010.04.010
8. Gong M, Chi C, Ye J, et al. Icariin-loaded electrospun PCL/gelatin nanofiber membrane as potential artificial periosteum. *Colloids Surf B Biointerfaces*. 2018;170:201–209. doi:10.1016/j.colsurfb.2018.06.012
9. Chen S, John JV, McCarthy A, et al. New forms of electrospun nanofiber materials for biomedical applications. *J Mater Chem B*. 2020;8(17):3733–3746. doi:10.1039/d0tb00271b
10. Yoo HS, Kim TG, Park TG. Surface-functionalized electrospun nanofibers for tissue engineering and drug delivery. *Adv Drug Deliv Rev*. 2009;61(12):1033–1042. doi:10.1016/j.addr.2009.07.007
11. Anup N, Chavan T, Chavan S. Reinforced electrospun nanofiber composites for drug delivery applications. *J Biomed Mater Res A*. 2021;109(10):2036–2064. doi:10.1002/jbm.a.37187
12. Tawfik EA, Craig DQM, Barker SA. Dual drug-loaded coaxial nanofibers for the treatment of corneal abrasion. *Int J Pharm*. 2020;581:119296. doi:10.1016/j.ijpharm.2020.119296
13. Chen X, Li H, Lu W, et al. Antibacterial porous coaxial drug-carrying nanofibers for sustained drug-releasing applications. *Nanomaterials*. 2021;11(5):1316–1328. doi:10.3390/nano11051316
14. Peng W, Ren S, Zhang Y, et al. MgO nanoparticles-incorporated PCL/gelatin-derived coaxial electrospinning nanocellulose membranes for periodontal tissue regeneration. *Front Bioeng Biotechnol*. 2021;9:668428. doi:10.3389/fbioe.2021.668428
15. Khan AUR, Huang K, Khalaji MS, et al. Multifunctional bioactive core-shell electrospun membrane capable to terminate inflammatory cycle and promote angiogenesis in diabetic wound. *Bioact Mater*. 2021;6(9):2783. doi:10.1016/j.bioactmat.2021.01.040
16. Ren X, Hu Y, Chang L, Xu S, Mei X, Chen Z. Electrospinning of antibacterial and anti-inflammatory Ag@hesperidin core-shell nanoparticles into nanofibers used for promoting infected wound healing. *Regen Biomater*. 2022;9:rbac012. doi:10.1093/rb/rbac012

17. Tavakoli M, Mirhaj M, Salehi S, et al. Coaxial electrospun angiogenic nanofiber wound dressing containing advanced platelet rich-fibrin. *Int J Biol Macromol*. 2022;222:1605–1618. doi:10.1016/j.ijbiomac.2022.09.109
18. Han D, Steckl AJ. Coaxial electrospinning formation of complex polymer fibers and their applications. *ChemPlusChem*. 2019;84(10):1453–1497. doi:10.1002/cplu.201900281
19. Zhuang W, Yue L, Dang X, et al. Rosenroot (Rhodiola): potential applications in aging-related diseases. *Aging Dis*. 2019;10(1):134–146. doi:10.14336/AD.2018.0511
20. Dai Z, Zhang X, Li W, et al. Salidroside induces apoptosis in human gastric cancer cells via the downregulation of ENO1/PKM2/GLUT1 expression. *Biol Pharm Bull*. 2021;44(11):1724–1731. doi:10.1248/bpb.b21-00443
21. Zheng X-T, Wu Z-H, Wei Y, et al. Induction of autophagy by salidroside through the AMPK-mTOR pathway protects vascular endothelial cells from oxidative stress-induced apoptosis. *Mol Cell Biochem*. 2017;425(1–2):125–138. doi:10.1007/s11010-016-2868-x
22. Zhang Y, Lu W, Zhang X. Cryptotanshinone protects against pulmonary fibrosis through inhibiting Smad and STAT3 signaling pathways. *Pharmacol Res*. 2019;147:104307. doi:10.1016/j.phrs.2019.104307
23. Wu JQ, Mao LB, Liu LF, et al. Identification of key genes and pathways of BMP-9-induced osteogenic differentiation of mesenchymal stem cells by integrated bioinformatics analysis. *J Orthop Surg Res*. 2021;1:273. doi:10.1186/s13018-021-02390-w
24. Maeda K, Kobayashi Y, Koide M. The regulation of bone metabolism and disorders by wnt signaling. *Int J Mol Sci*. 2019;20(22):5525. doi:10.3390/ijms20225525
25. Guo C, Liu R, Zhao H-B, Qin G-H. Wnt/β-catenin信号通路介导红景天苷诱导间骨髓充质干细胞向神经细胞定向分化研究 [Wnt/β-catenin signal pathway mediated Salidroside induced directional differentiation from mouse mesenchymal stem cells to nerve cells]. *Zhongguo Zhong Xi Yi Jie He Za Zhi*. 2015;35(3):349–354. Chinese.
26. Li X-H, Chen F-L, Shen H-L. Salidroside promoted osteogenic differentiation of adipose-derived stromal cells through Wnt/β-catenin signaling pathway. *J Orthop Surg Res*. 2021;16(1):456. doi:10.1186/s13018-021-02598-w
27. Wang Y, Han J, Luo L, Kasim V, Wu S. Salidroside facilitates therapeutic angiogenesis in diabetic hindlimb ischemia by inhibiting ferroptosis. *Biomed Pharmacother*. 2023;159:114245. doi:10.1016/j.biopha.2023.114245
28. Xq G, L Q, J Y, et al. Salidroside accelerates fracture healing through cell-autonomous and non-autonomous effects on osteoblasts. *Cell Tissue Res*. 2017;367(2):197–211. doi:10.1007/s00441-016-2535-2
29. Yang W, Han J, Gong S, Zhao J, Yu T, Ma J. Cryptotanshinone suppressed postmenopausal osteoporosis by preventing RANKL-mediated osteoclastogenesis against kidney injury. *Evid Based Complement Alternat Med*. 2022;2022:2821984. doi:10.1155/2022/2821984
30. Liu J, Wu S, Ma J. Polycaprolactone/gelatin/hydroxyapatite electrospun nanomembrane materials incorporated with different proportions of attapulgite synergistically promote bone formation. *Int J Nanomed*. 2022;17:4087–4103. doi:10.2147/IJN.S372247
31. Mahmood SK, Zakaria MZAB, Razak ISBA. Preparation and characterization of cockle shell aragonite nanocomposite porous 3D scaffolds for bone repair. *Biochem Biophys Rep*. 2017;10:237–251. doi:10.1016/j.bbrep.2017.04.008
32. Rasool A, Ata S, Islam A. Stimuli responsive biopolymer (chitosan) based blend hydrogels for wound healing application. *Carbohydr Polym*. 2019;203:423–429. doi:10.1016/j.carbpol.2018.09.083
33. Li Y, Xu P, He D, et al. Long-circulating thermosensitive liposomes for the targeted drug delivery of oxaliplatin. *Int J Nanomed*. 2020;15:6721–6734. doi:10.2147/IJN.S250773
34. Zhang W, Xue D, Yin H, et al. Overexpression of HSPA1A enhances the osteogenic differentiation of bone marrow mesenchymal stem cells via activation of the Wnt/β-catenin signaling pathway. *Sci Rep*. 2016;6(1):27622. doi:10.1038/srep27622
35. Kim H-W, Knowles JC, Kim H-E. Hydroxyapatite and gelatin composite foams processed via novel freeze-drying and crosslinking for use as temporary hard tissue scaffolds. *J Biomed Mater Res A*. 2005;72(2):136–145. doi:10.1002/jbm.a.30168
36. Gautam S, Chou C-F, Dinda AK, Potdar PD, Mishra NC. Surface modification of nanofibrous polycaprolactone/gelatin composite scaffold by collagen type I grafting for skin tissue engineering. *Mater Sci Eng C Mater Biol Appl*. 2014;34:402–409. doi:10.1016/j.msec.2013.09.043
37. Martins-Franchetti SM, Egerton TA, White JR. Morphological changes in poly(caprolactone)/poly(vinyl chloride) blends caused by biodegradation. *J Polym Environ*. 2010;18(1):79–83. doi:10.1007/s10924-009-0158-3
38. Qian Y, Zhou X, Zhang F, et al. Triple PLGA/PCL scaffold modification including silver-impregnation, collagen-coating, and electrospinning significantly improve biocompatibility, antimicrobial, and osteogenic properties for oro-facial tissue regeneration. *ACS Appl Mater Interfaces*. 2019;11(41):37381. doi:10.1021/acsami.9b07053
39. Gautam S, Sharma C, Purohit SD. Gelatin-polycaprolactone-nanohydroxyapatite electrospun nanocomposite scaffold for bone tissue engineering. *Mater Sci Eng C Mater Biol Appl*. 2021;119:111588. doi:10.1016/j.msec.2020.111588
40. Campos LD, Santos Junior VDA, Pimentel JD, Carregã GLF, Cazarin CBB. Collagen supplementation in skin and orthopedic diseases: a review of the literature. *Heliyon*. 2023;9(4):e14961. doi:10.1016/j.heliyon.2023.e14961
41. Shuai C, Shi X, Yang F, et al. Oxygen vacancy boosting Fenton reaction in bone scaffold towards fighting bacterial infection. *Int J Extre Manufact*. 2023;1:6.
42. Feng P, Wang K, Shuai Y, et al. Hydroxyapatite nanoparticles in situ grown on carbon nanotube as a reinforcement for poly (ε-caprolactone) bone scaffold. *Mater Today Adv*. 2022;15:100272. doi:10.1016/j.mtadv.2022.100272
43. Kumar N, Saraber P, Ding Z, Kusumbe AP. Diversity of vascular niches in bones and joints during homeostasis, ageing, and diseases. *Front Immunol*. 2021;12:798211. doi:10.3389/fimmu.2021.798211
44. Lafage-Proust MH, Prisby R, Roche B, Vico L. Bone vascularization and remodeling. *Joint Bone Spine*. 2010;77(6):521–524. doi:10.1016/j.jbspin.2010.09.009
45. Mu C, Hu Y, Hou Y. Substance P-embedded multilayer on titanium substrates promotes local osseointegration via MSC recruitment. *J Mater Chem B*. 2020;8(6):1212–1222. doi:10.1039/C9TB01124B
46. Guo Q, Yang J, Chen Y. Salidroside improves angiogenesis-osteogenesis coupling by regulating the HIF-1α/VEGF signalling pathway in the bone environment. *Eur J Pharmacol*. 2020;884:173394. doi:10.1016/j.ejphar.2020.173394
47. Cristina C, Perez-Millan MI, Luque G. VEGF and CD31 association in pituitary adenomas. *Endocr Pathol*. 2010;21(3):154–160. doi:10.1007/s12022-010-9119-6
48. Kasprzak A, Surdacka A, Tomczak M. Expression of angiogenesis-stimulating factors (VEGF, CD31, CD105) and angiogenetic index in gingivae of patients with chronic periodontitis. *Folia Histochem Cytobiol*. 2012;50(4):554–564. doi:10.5603/20324